

A theoretical and experimental study of cell membrane  
electrostatics and transport

Vasiliki–Christina Panagiotopoulou

November 9, 2012

Thesis to be submitted to the University of Nottingham for the degree of Master of  
Philosophy

# Contents

<b>1</b>	<b>Introduction</b>	<b>7</b>
1.1	Multidrug resistance . . . . .	7
1.2	Cell biology and electrostatic modelling . . . . .	8
1.2.1	Biology of the cell . . . . .	8
1.2.2	Basic principles of electrostatics . . . . .	12
1.3	Experimental techniques and findings on membrane potential alterations . . . . .	16
1.4	Stochastic models of biological systems . . . . .	20
1.5	Aims of the present work . . . . .	21
<b>2</b>	<b>Experimental materials, methods and results</b>	<b>22</b>
2.1	Introduction . . . . .	22
2.2	Methods . . . . .	22
2.2.1	Materials . . . . .	22
2.2.2	Cell culture . . . . .	23
2.2.3	Preparation of solutions . . . . .	23
2.2.4	Cell preparation . . . . .	24
2.2.5	Measuring fluorescence . . . . .	24

2.3	Experimental results . . . . .	25
2.4	Conclusions . . . . .	34
<b>3</b>	<b>Modelling the electrostatic properties of a single cell as a response to pH changes</b>	<b>35</b>
3.1	Nondimensionalization . . . . .	40
3.2	Linearization . . . . .	43
3.3	Non linear solutions . . . . .	47
3.4	Results of electrostatic modelling . . . . .	52
<b>4</b>	<b>Modelling the experimental results</b>	<b>56</b>
4.1	Valinomycin modelling . . . . .	56
4.2	Potential modelling . . . . .	61
4.3	Conclusions from modelling the experimental procedures . . . . .	66
4.3.1	Modelling valinomycin . . . . .	66
4.3.2	Potential modelling . . . . .	67
<b>5</b>	<b>CONCLUSIONS</b>	<b>71</b>

## ABSTRACT

In cancer, neoplastic cells can develop resistance to a variety of drugs, even to those drugs that cells have never come across. This makes the cancer therapy even more demanding and challenging, as clinicians have to take into consideration that the heavy medication they administer to the patients can be ineffective. This phenomenon acts as a motivation to explore the mechanisms behind molecular transport across the cell membrane. Using cancer cells and fluorescent dyes, we can detect experimentally whether a dye molecule can enter the cell. The most important aim of this research work is to detect whether there is a link between physical parameters of the cell, like the membrane charge density and the ionic accumulation, and the molecule's transport. We then build a mathematical model to explain and predict what happens during the experimental procedure. Our experiments show that the dye's crossing is influenced by alteration of the membrane potential. In details, when the difference in potential across the membrane increases, then more dye molecules cross the membrane. Using our mathematical approach, we approximate the dye crossing the cell membrane via competition between diffusion and electrostatic forces. In that way, we are able to predict a molecule's movement from the outside to the inside of the cell when the potential, the distribution of ions and the electrostatic properties of the membrane are known. Furthermore, it is possible to predict the transport time of the molecule as well as its distribution in the vicinity of the membrane area.

## ACKNOWLEDGEMENTS

*As you set out for Ithaka  
hope the voyage is a long one ,  
full of adventures, full of discovery.*

*C. P. Cavafis*

*(translated by Ed. Keeley/ Ph. Sherrard)*

This work was performed at the School of Mathematical Sciences and the School of Veterinary Medicine and Science of Nottingham University, funded by Marie Curie Early Stage Training Fellowship (for the first two years) and by the School of Mathematical Sciences (for the last seven months). During this time, I met and worked with some wonderful people who I would like to mention them here and thank them once more.

First and most important of all, I would like to thank my supervisor, Professor Oliver E. Jensen who has helped me from day one. Along him I learnt that organization and thorough explanation of the scientific work produced are as vital as the work itself. I believe myself lucky to have worked with him.

Also I would like to thank Dr Cyril Rauch, my co-supervisor from the School of Veterinary Medicine and Science, who guided me into the Physics and Experiments world.

This list would not be complete if I don't mention Professor Helen Byrne and Dr Kostas Soldatos, both served as my internal assessors. Their remarks were decisive for the result of my work. Also, I would like to thank Dr Sarah Waters, my external assessor for her time committed to my thesis and her recommendations.

During my stay in UK, I asked for help far too many times Ms Helen Cunliffe, Ms Andrea Blackburn and Ms Hillary Londale. I just couldn't thank them enough for their patience.

Lastly, many thanks to my family and friends for being there while I was struggling with my “Lastrigonians and Cyclops, angry Poseidon” through my journey to “Ithaca”.

# 1 Introduction

This is an introductory chapter that contains a literature review covering every aspect of this work featured in the thesis. The initiative of this work was multidrug resistance which is described in section 1.1. Section 1.2 is dedicated to cell biology and electrostatic modelling. In section 1.2.1 basic knowledge on cell biology is outlined, followed by a brief timeline on the modelling of electrostatics (section 1.2.2) which underpins theory described in Chapter 3. Section 1.3 describes the biology behind the experimental techniques described in Chapter 2, combined with results from similar experiments. The final section of the introduction (1.4) presents information about stochastic modelling in biological systems.

## 1.1 Multidrug resistance

According to NHS records, cancer is a major health issue in the UK, since “one in three people will be diagnosed with cancer in their lifetime, one in four will die of cancer” (<http://www.nhs.uk>). The situation becomes complicated since four out of ten human tumours develop drug resistance [82]. In the United States alone, drug-resistant tumours result in 500,000 deaths per year [82]. This observation is supported by numerous reports [5, 10, 12, 19, 23, 28, 29, 34, 37, 40, 44, 47, 48, 49, 50, 51, 55, 59, 66, 67, 75, 82, 83, 91, 93, 94, 95] which suggest that some types of neoplastic cells resist known chemotherapeutic drugs.

Patients during the post-surgical period or their in-hospital stay have a high risk of suffering from infections. One of the most frequent and serious infections is MRSA (Methicillin Resistant Staphylococcus Aureus). MRSA affects more than 300 out of 1,000,000 people [65], while 20 per cent of these cases prove fatal. The drugs used against MRSA have limited effect, making prevention the best treatment [65].

Resistance to drugs is also found in malaria parasites against antimalarials, in bacteria against a broad spectrum of antibiotics, even in plant cells against herbicides [7, 34, 47, 57, 67, 68, 71, 82, 91]. All these examples are part of a phenomenon known as Multidrug Resistance (MDR). MDR is a frequent problem, since it is common to a large group of prokaryotic and eukaryotic cells [47].

MDR motivates the work presented here. According to published theoretical and experimental work [5, 6, 7, 10, 19, 25, 29, 34, 36, 40, 48, 50, 51, 54, 55, 57, 67, 75, 76, 77, 78, 81, 82, 83, 85, 91, 93, 92, 94, 95], MDR is suspected to be connected (directly or indirectly is yet to be identify) to the membrane potential, the intracellular pH and the lipid distribution of affected cells.

Our goal is to identify the relationship between membrane potential, membrane charge and pH for a single cell and to understand the pathway of a molecule from outside the cell to the inside when subjected to different membrane potentials. We pursue this using a combination of experimental and theoretical approaches.

## **1.2 Cell biology and electrostatic modelling**

### **1.2.1 Biology of the cell**

The cell is the basic unit for all biological organisms. It contains vital information and provides substances for the survival of the organism. Because of its importance, the cell needs protection from the surrounding environment. This role is performed by the cell membrane. The membrane acts as a physical boundary separating the cell from its environment. The membrane is selectively permeable, allowing the crossing of certain molecules. This works in two ways, when the membrane functions properly; only the molecules that the cell needs are able to cross the membrane, while toxic compounds remain outside. Moreover the membrane is responsible for the communication of the cell with other cells [39].

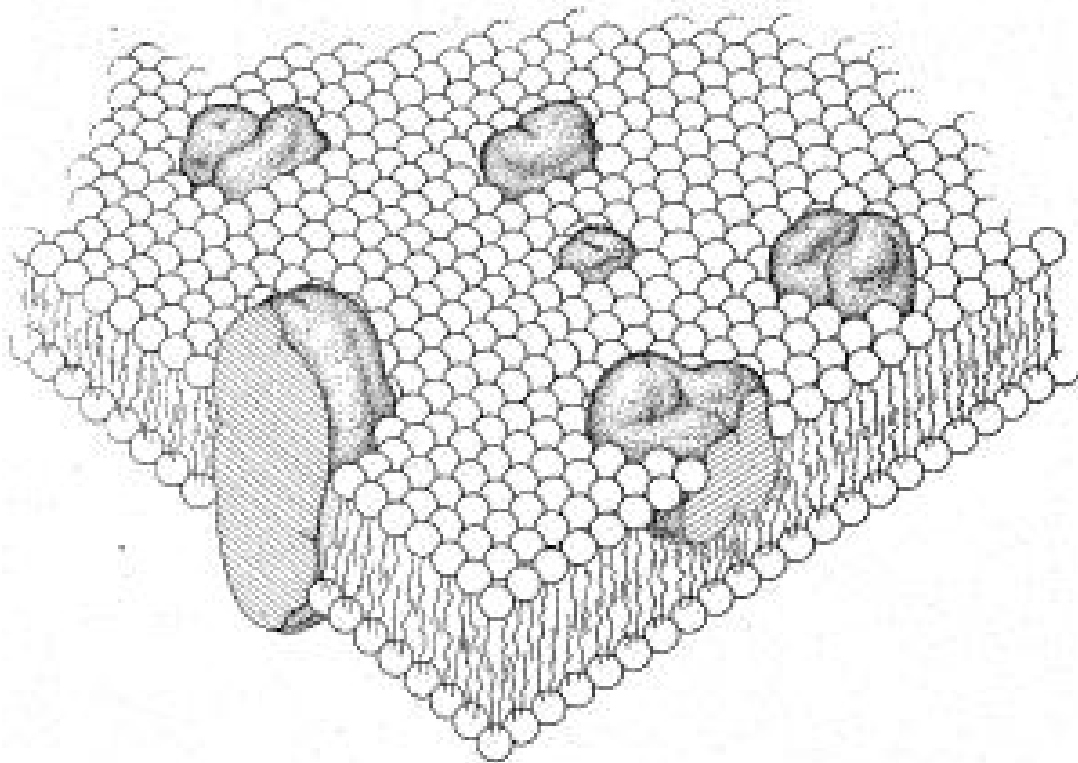


Figure 1: Part of the phospholipid bilayer as described in the Fluid Mosaic Model [98], where the circles represent the hydrophilic part of the phospholipids, the lines between the circles the lipophilic part of the phospholipids and the large structures the proteins.

Most cell membranes consist of a double bilayer of phospholipids with embedded proteins (Figure 1). This lipid bilayer is a continuous structure. The outer part of the bilayer, which contacts water, is ionic. The core of the bilayer is hydrophobic [39]. The membrane core is normally free of charge, whereas the outer parts of the membrane have charged phospholipids with an overall negative charge density of around  $0.05 \text{ C/m}^2$  [11]. The volume, size and charge of phospholipids, along with their distribution on either side of the bilayer, have an effect on the shape of the membrane because of electrostatic repulsion and attraction forces [90].

On the other hand, proteins are arranged discontinuously at the membrane. They can either bind to the membrane or cross the membrane. In some cases, proteins are freely soluble in the cytoplasm [39]. The thickness of the membrane varies but its average value is  $7.5 \text{ nm}$  [39]. The membrane structure is interrupted by pores. Some pores are filled with water, while others are lined with proteins and allow the crossing of specific compounds [39]. The latter are called “channels” [90].

Inside and outside the cell, there is a dilute aqueous solution of salts, especially containing sodium chloride (NaCl) and potassium chloride (KCl), which can be found dissociated into  $\text{Na}^+$ ,  $\text{K}^+$  and  $\text{Cl}^-$  ions. The membrane prevents the free flow of these ions in or out of the cell. Ions can cross the membrane when subjected to diffusive and electrical forces. The different values of concentrations create a potential difference across the membrane. For this reason, the cell membrane is usually modelled as a capacitor in parallel with an ionic current, using basic electrostatic models [39] (Figure 2).

The membrane is a complicated biological system in terms of electrostatics because of its ability to self-regulate and re-establish equilibrium. For these reasons, we use basic electrostatic equations to approximate the cellular mechanisms. These equations are described in the following sections.

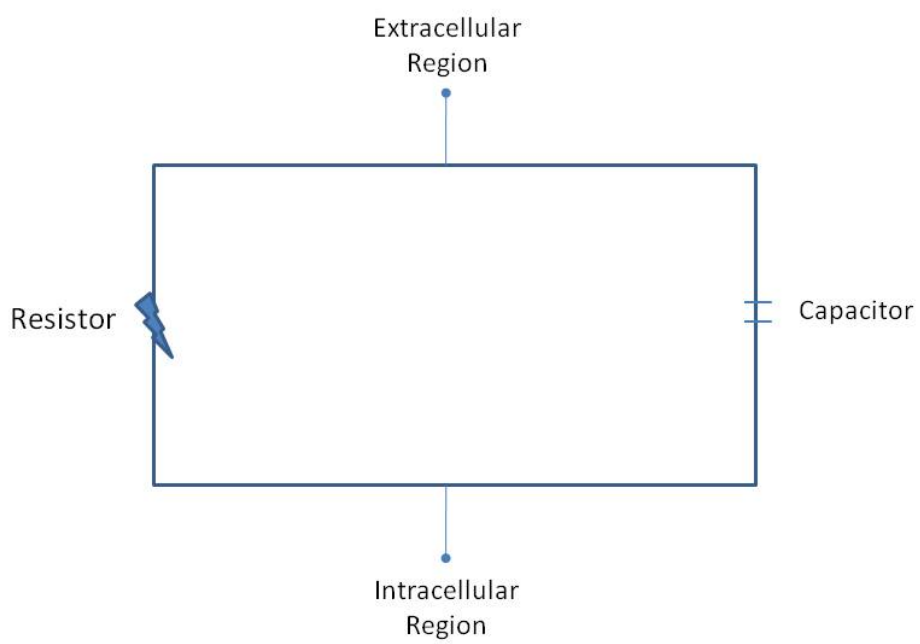


Figure 2: Capacitor-Resistor Model of the Membrane [39]

### 1.2.2 Basic principles of electrostatics

Research in electrostatics dates back to the 19th century. In 1800, Volta experimented on an electrode–electrolyte interface and managed to produce an electrical potential and thus to study direct current electricity [104]. Twenty–six years later, Ohm decided to change the Voltaic battery and, by experimenting on his new battery, he discovered the electrostatic law that bears his name [63]. It was not until 1834 that Faraday introduced the term “electrode” to describe the metallic plate used in electrostatic experiments [17]. In 1871, Varley [103] was the first to measure the capacitance of an interface while eight years later Helmholtz [33] was the first to model the electrode–electrolyte interface. He proposed [33] that a double layer of charge exists at the interface (Figure 3). This layer would be able to act as a charged capacitor, separating charges on either side of the membrane [33]. Nernst [61] and Brunner [8, 9] studied the problem of steady conductivity between parallel flat electrodes.

Gouy in 1910 suggested that the excess charge in the solution near an electrode can be viewed as a capacitance [30]. Both Gouy [30] and Chapman [13] suggested how a layer of charge may be smeared uniformly over a planar surface immersed in an electrolyte solution. Note that we use the term “Gouy–Chapman model” when referring to the model based on a set of advection–diffusion equations (also termed the Nernst–Planck equations, see equation (1) below), one for each ion species, coupled to the Poisson equation (equation 2) for the electric potential [80]. This model suggests that the total amount of charge is balanced out mostly by the distribution of counterions (ions of the opposite sign of the electrode) and less by the reduction of co–ions (ions of the same sign with the electrode) [88]. This results in non–negligible errors when assuming an asymmetrical electrolyte (the number of one ion species is larger than the other) to be symmetric (the number of anions equals the number of cations).

In 1924, Stern [101] realized that modelling electrolyte ions as point charges

was unsatisfactory. Thus, he introduced the Stern layer (Figure 3) between the inner and the outer planes that Helmholtz had introduced in this own model [33]. In the Helmholtz planes the charge and the potential distribution are assumed to increase linearly as we approach the membrane from its outer part. There is also a diffusion layer further from the electrode where the Gouy–Chapman model is applied. The “compact” layers (Helmholtz planes) can be found within a molecular distance of the surface, whereas the “diffuse” part (Gouy–Chapman) is extended into the solution at the scale of screening length (Figure 3). Physically the compact layer is intended to describe ions (at the outer Helmholtz plane) where solution molecules are in contact with the surface, although specifically absorbed ions may be also included [3]. Zimmerman (1930) experimented on, and provided proofs on, the effect of electrolyte concentration on the capacitance and the resistance of the electrode–electrolyte interface [110]. This work was followed by a model presented by Murdock and Zimmerman [60]. Later, Grahame refined the “Stern” model for the capacitance of the compact layer by performing his own experiments [31].

We now present the basic equations of the Gouy–Chapman model for an electrolyte containing a cation and an anion species, between two parallel and planar electrodes which are located  $x^* = \pm L$  [80]. Note that  $x^*$  is the axis perpendicular to the planar electrodes, whereas  $2L$  is the distance between them. At the surface of the capacitor, a reaction takes place where one or both ion species are produced and/or consumed. The Nernst–Planck expression for the ions is

$$\frac{\partial C^\pm}{\partial t} = -D^\pm \left( \frac{\partial C^\pm}{\partial x^*} \pm \frac{F}{RT} C^\pm \frac{\partial \phi^*}{\partial x^*} \right) \quad (1)$$

where  $\pm$  stand for the cation and the anion respectively,  $C^\pm$  for the concentration,  $t$  for time,  $D^\pm$  for the diffusion coefficient of the ions,  $\phi^*$  for the electric potential,  $F$  for the Faraday constant,  $R$  for the ideal gas constant and  $T$  for the absolute temperature.

The Poisson equation for the electric potential is described as

$$-\varepsilon^* \frac{d}{dx^*} \left( \frac{d\phi^*}{dx^*} \right) = z_e (C^+ - C^-) \quad (2)$$

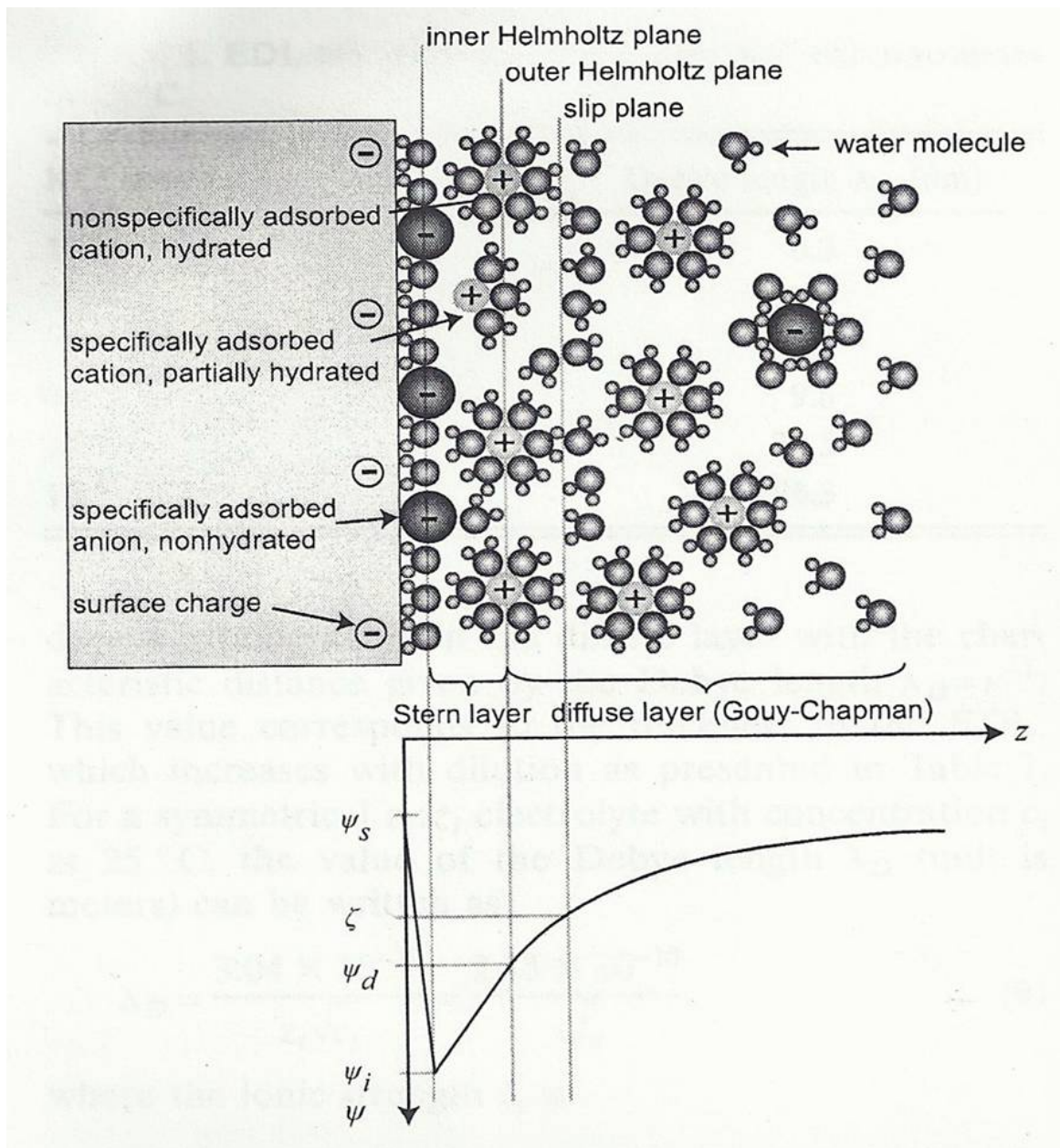


Figure 3: Gouy–Chapman model of the solid–electrolyte interface describing the potential vs. the distance from the wall of the capacitor. The inner Helmholtz plane consists of non hydrated ions, while the outer Helmholtz plane consists of hydrated counterions only. The diffuse layer starts from the outer Helmholtz layer. The Stern layer is found between the two Helmholtz planes [89].

where  $\varepsilon^*$  is the electric permittivity and  $z_e$  the ionic valence.

The Nernst–Einstein relation has been used in (1) as

$$D^\pm = RTu_\pm , \quad (3)$$

where  $u_\pm$  stands for the mobility of the ion. In the steady state case, there is no ionic flux,

$$-D^\pm \left( \frac{\partial C^\pm}{\partial x^*} \pm \frac{F}{RT} C^\pm \frac{\partial \phi^*}{\partial x^*} \right) = 0 . \quad (4)$$

At large distances from the electrodes, the concentrations of ions reach a constant value

$$C^+ \rightarrow C^{\infty+} , \quad (5)$$

$$C^- \rightarrow C^{\infty-} . \quad (6)$$

where  $C^{\infty+}$ ,  $C^{\infty-}$  are the concentrations for the cation and the anion respectively at the far fields, meaning really far from the membrane layers.

Depending on the assumptions used for this set of equations, various authors have derived analytical equations for simple cases and numerical approximations for more complex models [2, 11, 21, 20, 24, 52, 56, 64, 79, 84, 88, 96, 97].

As stated in section 1.2.1, the cell membrane resembles a capacitor (Figure 2). Most membrane models use a Poisson equation to describe the attraction of counterions to the membrane surface coupled to a Boltzmann equation to describe the attraction and repulsion forces between electrolyte ions and surface charges. To describe the ionic distribution in the electrolyte solution we use the Nernst equation [24, 52, 79, 97]. The models use different approaches depending on whether the dielectric constant of the electrolyte is uniform or not [2, 11, 39], whether the charges on the membrane are uniformly smeared over the planar membrane [2, 11, 20, 21, 56] or whether the ions in the electrolyte are point charges [2, 11, 56].

The most widely known model is the Gouy–Chapman model (1,2). For the cell membrane case, we assume that the membrane charges are smeared uniformly over

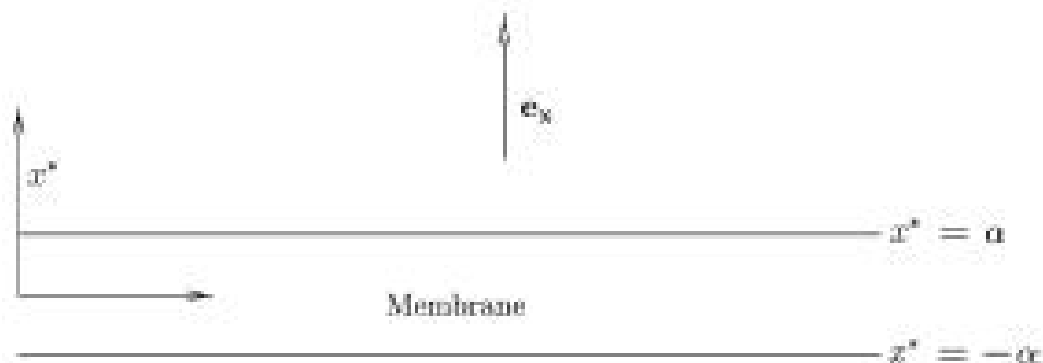


Figure 4: Schematic figure of the membrane where  $2\alpha$  is the width of the membrane[79], where the upper part is the inside of the cell and the lower part is the extracellular environment.

the membrane surface, the electrolyte solution is a structureless medium with a constant dielectric coefficient and the ions in the electrolyte solution are point charges [56]. It is the simplest possible model for the electrolyte solution but it works as documented by experimental data [56, 99].

For an electrolyte solution with an anion and a cation species near the cell membrane, we use equation (1), combined with equation (2) for the potential distribution.

This section provided a brief literature for the cell electrostatics. In the next section, we will present information about the mechanisms and the chemicals of the experiments, conducted as part of this study.

### 1.3 Experimental techniques and findings on membrane potential alterations

We are interested in understanding the way dyes accumulate within the cell. Measuring the membrane potential by using molecular probes is a rather common experiment. There are numerous studies measuring membrane potential in different kinds of cells [4, 15, 16, 18, 19, 26, 27, 36, 41, 43, 45, 51, 53, 72, 105, 109]. All these experiments conclude that increased fluorescence intensity of the dye results from

increased intracellular accumulation of the dye which is enhanced by the depolarization of the membrane.

Because of the ability of the cell membrane to serve as a barrier, the crossing of molecules via the membrane is described as either active or passive. By active, we refer to an energy-driven process, whereas passive crossing is energy-free as a direct effect of molecules' movement [39] (relying only on thermal fluctuations driving Brownian motion). Adding valinomycin in the cell environment is a passive way of promoting potassium ions crossing the cell membrane [15, 16, 25, 35, 36, 39, 100, 105, 106].

Valinomycin (Val) is a selective carrier for potassium ions produced by the bacterium *Streptomyces fulvissimes*. It is a circular molecule of molecular weight 1111.3 with six oxygen atoms on the inside to which a potassium ion binds. Figure 5 represents the structure of valinomycin.

To explain why valinomycin is selective to potassium ions rather than sodium ions, we note that both ions are in a water-based environment. Both ions, because of their positive charge, attract water molecules forming a protective shell around the cations. When the cations meet valinomycin, they interact with the six interior oxygen atoms which replace the water molecules of hydration. The fact that sodium is smaller than potassium hinders the interaction between sodium and all six oxygen atoms of valinomycin, whereas potassium is able to form a complex with valinomycin more easily. The interior of this complex is polar whereas the exterior surface is hydrophobic. This specific structure allows the molecule to enter the oily core of the membrane. When the complex encounters the membrane surface, the potassium separates from the complex. In other words, valinomycin enhances the flux of potassium cations depending on their concentration gradient [16, 35, 100].

Dye molecules are used to detect changes of the membrane potential [4, 15, 18, 27, 36, 41, 42, 43, 45, 46, 51, 53, 72, 105, 109]. In terms of experiments, membrane potential stands for the potential difference between the intra- and extra- cellular

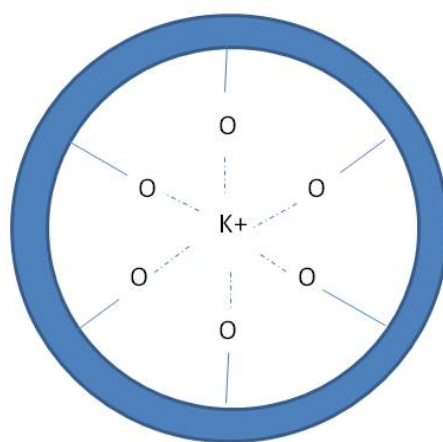


Figure 5: Complex of potassium–valinomycin, The ring represents the valinomycin carrier, while the O stand for the oxygen atoms that are on the inside of the carrier and  $K^+$  is an potassium ion [35].

aqueous phase. Membrane potential dyes are divided into two categories (slow or fast) based on the speed, size and mechanism of potential-dependent optical changes [4, 15, 27, 41, 45, 72, 105, 109].

Slow dyes, also known as “redistribution” or “Nernstian” dyes, respond to membrane potential changes in seconds, are permeant and work by a mechanism involving potential-dependent redistribution of the dye between the medium and the inside of the cell, organelle or vesicle [4, 45, 72, 105]. In other words, slow dyes monitor membrane potential by moving across the membrane until they reach equilibrium. All slow dyes are membrane-permeable cationic or anionic fluorochromes with charge delocalized over the whole fluorochrome structure. This charge delocalization is undoubtedly a prerequisite for the high membrane permeability. The dye permeability can be modulated by structural features which influence its hydrophobicity [105]. Slow dyes include carbocyanines, oxonols and rhodamine derivatives.

Fast-response dyes respond to membrane potential changes in less than milliseconds. So far they have been used in numerous experiments. However there are certain limitations. They produce a rather modest signal for most fluorescent sensors, so it is necessary to synthesize more sensitive potential probes. Also, because of the intense illumination they exhibit, many cells could be damaged. This damage is often a result from the interaction of excited dye molecules with oxygen to form singlet oxygens, which in turn leads to the production of free radicals that react with the membrane components [4, 72, 105].

In order to fully understand and model experimental conditions, we use stochastic equations due to the noise and the “vulnerability” of the system to changes. The literature for this approach is described in the next section.

## 1.4 Stochastic models of biological systems

Many scientists [14, 22, 58, 62, 73, 86, 87, 107] use stochastic equations to model biological systems with noise. There are several significant similarities between biological processes and stochastic theory that allow the use of this approach.

An important consideration is Brownian motion [102]. A Brownian particle in a fluid environment performs a lot of small and uncorrelated jumps [102]. In macroscopic terms, it is not the movement of one Brownian particle that we observe but rather the average distribution of Brownian particles, provided that the particles do not interact with one another. These average features vary in ways that can be described by simple laws [102].

A molecule performing Brownian motion can be subject to two different movements; the one is guided by a concentration gradient and the other one is based on a field introduced by an external force [86, 87]. The concentration-guided motion gives a certain direction to the system, while the stochastic process affects the speed which the system requires to achieve the final state [87].

A Brownian particle is described by a Fokker-Planck equation

$$\frac{\partial P}{\partial t} = -\frac{\partial}{\partial x^*} \left[ \frac{F(x^*)}{M\gamma} P \right] + D \frac{\partial^2 P}{\partial x^{*2}}, \quad (7)$$

where  $P(x^*, t)$  is the probability density of the molecule to be found in given position  $x^*$  at time  $t$ ,  $F(x^*)$  is the force applied to the molecule,  $M$  is the molecular weight of the particle,  $D$  the diffusion coefficient of the molecule and  $\gamma$  the drag coefficient [102], when the variables of the system are continuous [87]. Note that  $Pdx$  is the probability of the dye being found in the interval  $(x^*, x^* + dx^*)$ .

Several cases of biological systems that have been treated with Fokker-Planck equation are brain activity [108], neural oscillators [38], enzymic cycles [87] and cell migration [86].

In section 4.2 we will use the Fokker-Planck equation to simulate the movement

of a molecule from outside of the cell to the inside. Next, we will present the outline of our work, plus a list of our aims.

## **1.5 Aims of the present work**

In the next chapters, we will describe the experiments (Chapter 2), which we combine with the mathematical interpretation of the biology (Chapter 3) and we are able to produce a theoretical model (Chapter 4) for predicting the distribution of molecules within a cell domain based on altering extracellular conditions.

Researching on MDR has triggered many questions about the way molecules, larger than ions, cross the membrane. Differences between drug-sensitive and drug-resistant cells in physical parameters, such as intracellular pH, membrane potential and lipid distribution on the membrane, suggest to researchers possible investigation areas. In our work, we focus on how a molecule can be distributed near the membrane when different concentrations of ions or different potential values apply. Moreover, we are interested in what happens when the hydrogen concentration (in other words, pH) is altered as pH is a useful and common parameter for biological experiments and procedures. To sum up, this work is aiming in defining the relation between molecule transport, potential alterations, different ionic concentrations and pH variation. This work will offer a start for a further examination of the links of MDR with the physical properties of the cell. The next section describes the experimental techniques and main results.

## 2 Experimental materials, methods and results

### 2.1 Introduction

In this chapter we focus on the experiments supporting this work. These experiments were performed by the writer to underline the interdisciplinarity of the Marie Curie Project that funded the studies. We used cells from a cancer cell line and altered their membrane potential by using chemicals to alter the potassium concentration inside the cell. These experiments were performed in order to check whether an alteration in the extracellular environment of the cell could affect the distribution of a potential sensitive dye. The data from the experiments generally confirm this hypothesis and allow its use in a generalized model.

### 2.2 Methods

#### 2.2.1 Materials

Bis-(1,3-dibutylbarbituric acid)-trimethine oxonol (DiSBAC<sub>4</sub>(3)) and valinomycin (Val) were purchased from Invitrogen and were used without any further purification. Sodium chloride (NaCl), potassium chloride (KCl), calcium chloride (CaCl<sub>2</sub>), magnesium chloride (MgCl<sub>2</sub>), glucose (C<sub>6</sub>H<sub>12</sub>O<sub>6</sub>) and 4-(2-hydroxyethyl)-1-piperazineethanesulfonic acid (HEPES) were supplied by the stock of the School of Veterinary Medicine and Science, University of Nottingham, where the experiments took place. A continuous drug-sensitive erythroleukemia cell line (K562) was provided by Dr C. Rauch. For cell culture, we used Roswell Park Memorial Institute media (RPMI) containing L-Glutamine and 25 mM of HEPES. We also purchased Phosphate Buffered Saline (PBS) from Invitrogen that was used during the cell preparation.

Potassium Solutions	Potassium Concentrations
SK1	4.5 mM
SK2	12 mM
SK3	50 mM
SK4	100 mM
SK5	164.5 mM

Table 1: SKi solutions with different potassium concentrations

### 2.2.2 Cell culture

K562 cells were grown in a solution of RPMI. They were stored in a continuous culture incubator at 37 °C and 5 % of CO<sub>2</sub> . They were passaged regularly to prevent them from forming aggregates and from coming in contact with the walls of the flask. They were handled in a vacuum and sterile hood in order to decrease the chances of contamination.

### 2.2.3 Preparation of solutions

Buffer solutions (labelled SK1 to SK5) were imposed as extracellular medium to the cells. We prepared five different buffer solutions with different concentrations of potassium (Table 1) and sodium chloride by keeping the overall amount of cations and anions constant in all solutions. Besides sodium and potassium chloride, we also added calcium chloride (0.11099 g in 500 mL of buffer solution) and magnesium chloride (0.04761 g in 500 mL of buffer solution), as well as glucose ( 0.9008 g in 500 mL of buffer solution) and HEPES (1.19155 g in 500 mL of buffer solution). All solutions were water-based. Valinomycin solution was prepared by diluting 25 mg of valinomycin powder in 3 mL of anhydrous dimethyl sulfoxide (DMSO). The dye solution was prepared by dissolving 1 mg of DiSBAC<sub>4</sub>(3) powder in 608  $\mu$ L of Dimethyl Sulfoxide (DMSO).

#### 2.2.4 Cell preparation

The procedure described below was performed five times, each time with a different buffer solution. For each buffer solution we repeated the procedures twice to avoid statistical errors. We will describe the procedure for one buffer solution, i.e. SKi (Table 1),  $i = 1, \dots, 5$ , as the same procedure was followed for the rest of the buffer solutions.

We used 350 mL of cells in culture medium and divided them in seven tubes, each one containing 50 mL of cell culture. After centrifugation at 1200 rpm for 10 minutes in culture medium, the remaining pellets were transferred in smaller tubes (ependorfs) shortly after the supernatant liquid was disposed. The cells were double washed in 1 mL of PBS, centrifuged for 30 seconds at 7.5 g and resuspended in 1 mL of PBS.

Each eppendorf containing cells was then labelled individually to supply a background sample, a control sample, a sample for measuring the effects of DMSO as the dye's solvent and the remaining four samples were used to check the effects of different amounts of valinomycin (1, 5, 10, 50  $\mu\text{g}$ ). Cells were then incubated for 20 minutes, followed by centrifugation at 1.2 rpm for 10 minutes, at the end of which PBS was washed away. In all eppendorfs we introduced 1 mL of SKi, except in the case of the background sample where we added 1 mL of PBS. Cell solutions were then transferred on a 96-well plate where 1 mL of cell solution was divided in five wells.

#### 2.2.5 Measuring fluorescence

Fluorescence intensity signals were obtained with a fluorometer (FLUOSTAR) connected to a DELL computer. The 96-well plate was loaded in the cavity of the fluorometer and DiSBAC<sub>4</sub>(3) was injected after 2 minutes of fluorescence activity. The temperature remained constant throughout the entire duration of the measure-

Sample Label	Signal Composition
sample 1	control signal-background signal
sample 2	DMSO effect signal-background signal
sample 3	SKi+Val1 signal-background signal
sample 4	SKi+Val5 signal-background signal
sample 5	SKi+Val10 signal-background signal
sample 6	SKi+Val50 signal-background signal

Table 2: Signal labels for samples, where SKi stands for a buffer solution, Val1 for 1  $\mu\text{g}$  of added valinomycin solution per 1 mL of sample, Val5 for 5  $\mu\text{g}$  of added valinomycin solution per 1 mL of sample, Val10 for 10  $\mu\text{g}$  of added valinomycin solution per 1 mL of sample and Val50 for 50  $\mu\text{g}$  of added valinomycin solution per 1 mL of sample.

ment. Cell suspensions were shaken regularly in order to prevent cells from sticking on the bottom of the well. The excitation filter was set at 485 nm and the emission filter at 590 nm.

### 2.3 Experimental results

Figures 6-10 show the measurements of fluorescence intensity for SK1–SK5 respectively. In order to be able to compare parameters, we have subtracted the background noise; the label of the samples is as described in Table 2.

In Figure 6, adding DMSO results in an increase of the fluorescent intensity signal compared to that of the control sample. This might be because the DMSO can destroy parts of the membrane when added in relatively large concentrations in the cell environment. So, if that’s the case here, the dye would cross the membrane far more easily and thus the intensity signal increases. In the case of SK1 as a buffer solution, the potassium concentration is smaller in the extracellular area (4.5 mM compared to 140 mM inside the cell according to literature [1]). When adding a small amount of valinomycin (1  $\mu\text{g}$  per mL), the signal seems smaller compared to the control one at first. In detail, when we add valinomycin we allow potassium ions to cross the membrane more easily which in this case causes potassium ions to

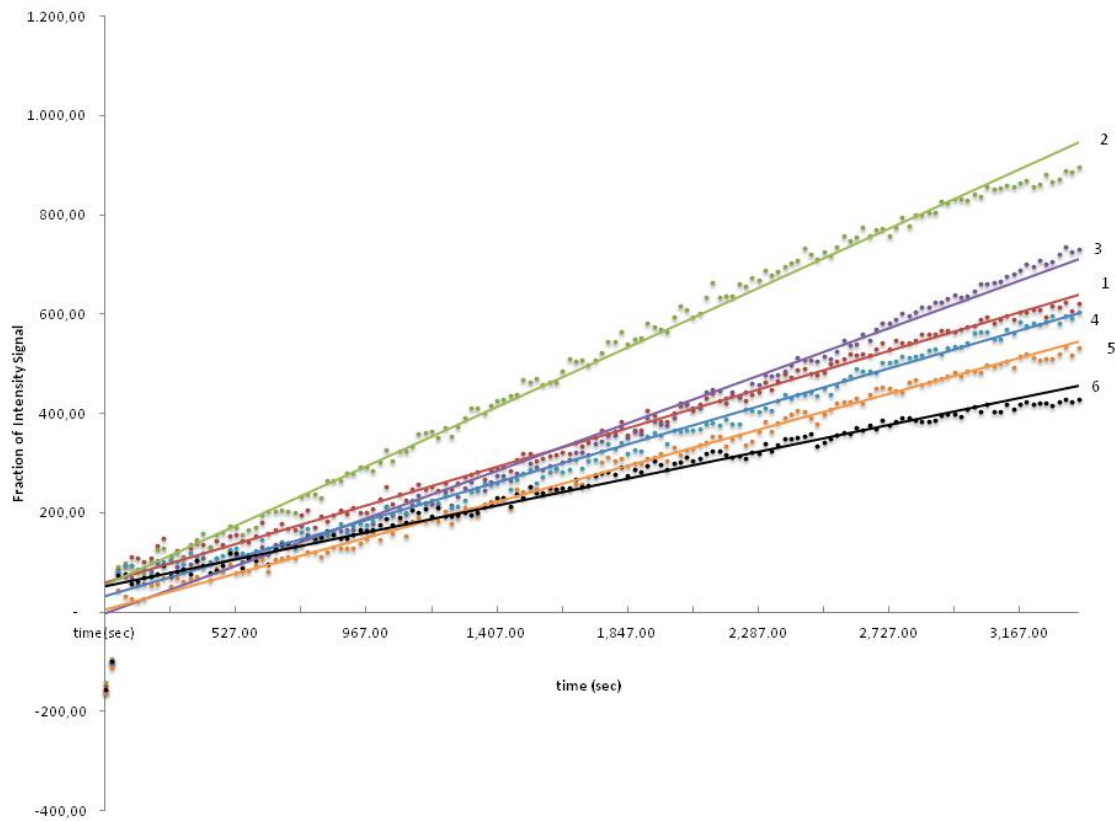


Figure 6: Fraction of fluorescence intensity signal when using SK1 with the samples being explained in table 2, where the red dots represent data from sample 1, green from sample 2, purple from sample 3, light blue from sample 4, orange from sample 5 and black from sample 6. The intensity signal is normalised by the intensity signal of the background sample, to avoid noise due to temporary conditions.

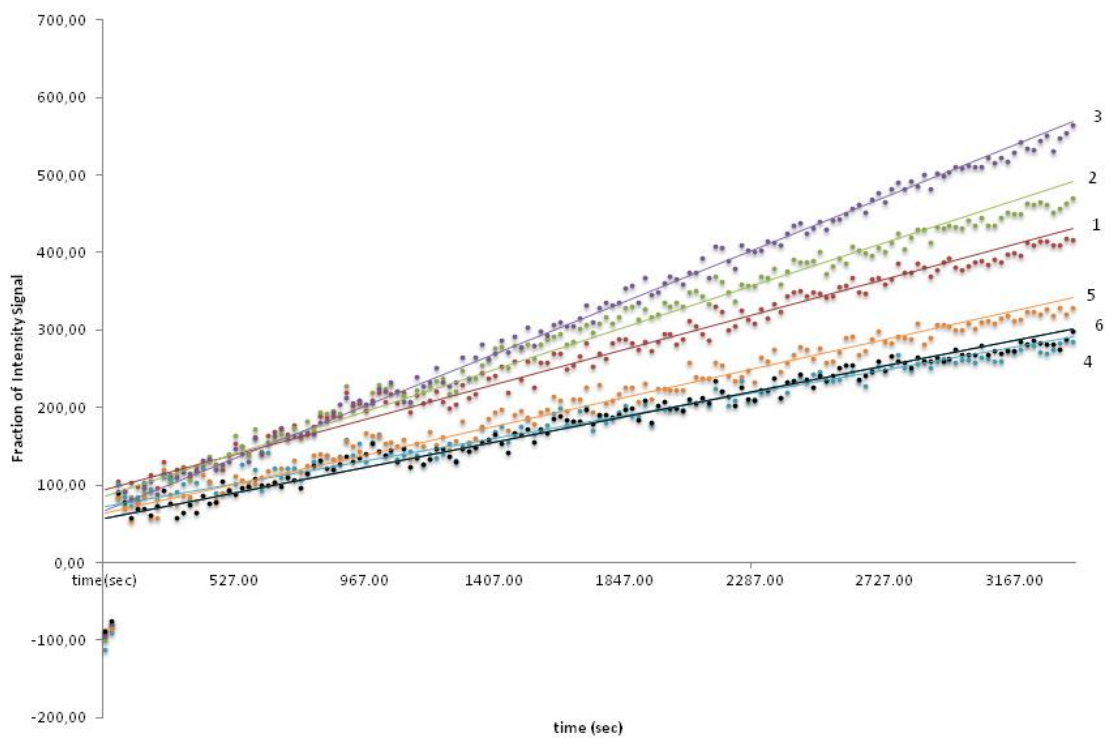


Figure 7: Fluorescence intensity signal when using SK2 with the samples being explained in table 2, where the red dots represent data from sample 1, green from sample 2, purple from sample 3, light blue from sample 4, orange from sample 5 and black from sample 6. The intensity signal is normalised by the intensity signal of the background sample, to avoid noise due to temporary conditions.

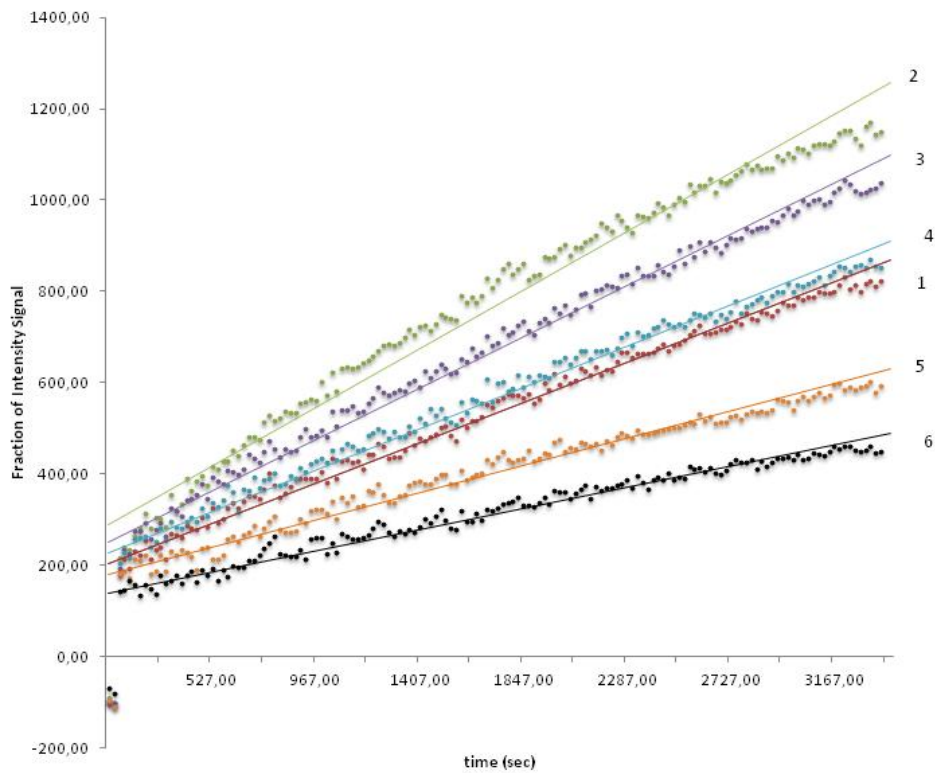


Figure 8: Fluorescence intensity signal when using SK3 with the samples being explained in table 2, where the red dots represent data from sample 1, green from sample 2, purple from sample 3, light blue from sample 4, orange from sample 5 and black from sample 6. The intensity signal is normalised by the intensity signal of the background sample, to avoid noise due to temporary conditions.

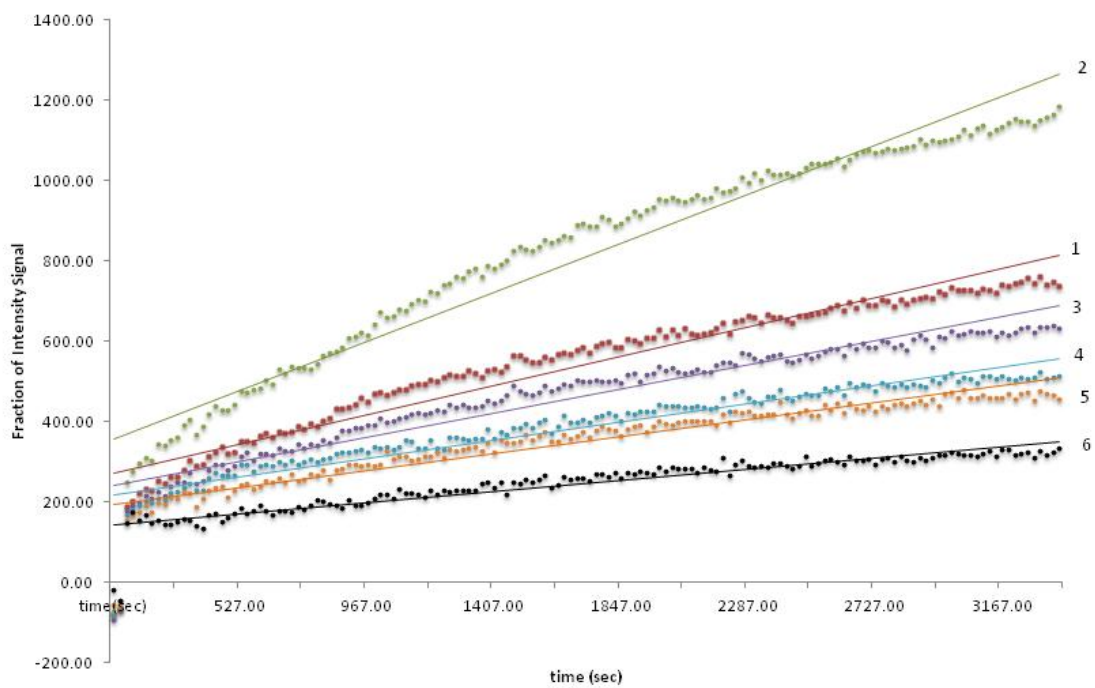


Figure 9: Fluorescence intensity signal when using SK4 with the samples being explained in table 2, where the red dots represent data from sample 1, green from sample 2, purple from sample 3, light blue from sample 4, orange from sample 5 and black from sample 6. The intensity signal is normalised by the intensity signal of the background sample, to avoid noise due to temporary conditions.

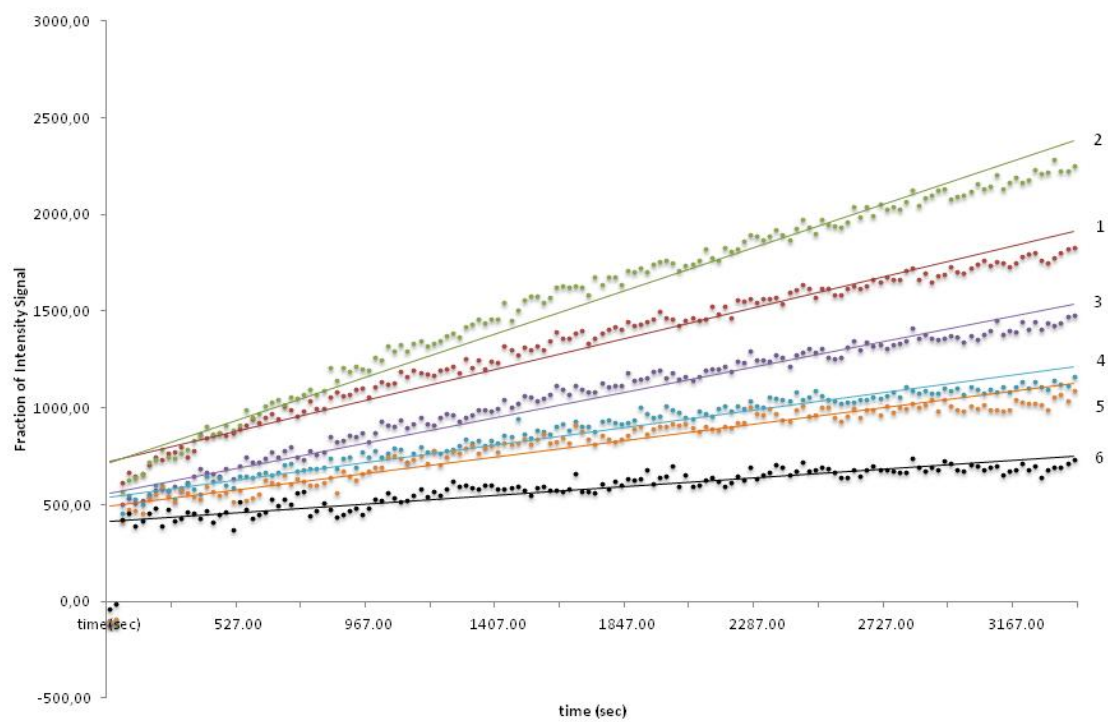


Figure 10: Fluorescence intensity signal when using SK5 with the samples being explained in table 2, where the red dots represent data from sample 1, green from sample 2, purple from sample 3, light blue from sample 4, orange from sample 5 and black from sample 6. The intensity signal is normalised by the intensity signal of the background sample, to avoid noise due to temporary conditions.

leave the cell. This tendency will make the crossing of dye molecules more difficult because of the electroneutrality disturbance. So, the signal will drop. However after some time, the absolute value of the signal from sample 3 is larger than the absolute value from sample 2 which may be caused by a higher rate of diffusion of the dye. Then, as we increase the amount of valinomycin added in the system, the signal gradually drops with the lowest signal being emitted by the sample with the largest amount of valinomycin.

In Figure 7, the extracellular concentration of potassium is closer to the concentration of potassium inside the cell, but still smaller. In this case due to unexpected laboratory conditions (the cells continue to duplicate throughout the day, plus the experimental error occurred when adding the chemicals) during the procedure, the graphs are not as straightforward as the rest of the graphs. But, generally, the sample with the lowest amount of valinomycin exhibits a higher signal than the sample with the highest amount of valinomycin added.

In Figure 8, the concentration of extracellular potassium ions increases further, so the tendency of potassium ions to cross the membrane from inside of the cell to the outside is expected to be slow down because of the smaller concentration gradient. The same trends as in Figure 6 confirm that the addition of Valinomycin to the system results in decrease of signal.

Figure 9 is a perfect example of the curves we are expecting from the experiment. The line from sample 2 is above the curve from sample 1. At the same time, adding valinomycin results in lower slopes for the curves from samples 3 to 6.

In Figure 10, the extracellular potassium concentration is larger than the concentration of the cation intracellularly. The valinomycin addition does not seem to result in as large changes as figures 6–9. Actually in this case, trends of the curves as described before are followed after a period of time when mechanisms of the cell begin to restore equilibrium and electroneutrality inside the cell. This is obvious, because up to approximately 500 seconds the curves for all samples are close to

Sample Label	SK1	SK2	SK3	SK4	SK5
sample 1	3.8918	2.2646	4.413	3.6328	7.9603
sample 2	5.9865	2.7248	6.4282	6.1079	11.158
sample 3	4.7807	3.371	5.6168	3.0008	6.5549
sample 4	3.8181	1.4677	4.526	2.286	4.5173
sample 5	3.6189	1.8712	2.9825	2.1119	4.2398
sample 6	2.7138	1.6337	2.321	1.3814	2.2567

Table 3: Dimensionless slope values from linear approximation of the curves from Figures 6-10.

each other. In particular, the curve of sample 2 has lower signal values than the curve of sample 1. This fact is contradictive to the theory already mentioned, but is explained with the idea of equilibrium restoration.

Although the different laboratory conditions during the experiments (different amount of cells per mL throughout the day due to mitosis, difference in concentration of chemicals due to the inability of tools to handle small amounts of chemicals) do not allow direct comparison between different experiments, for almost every buffer solution it is obvious that the rate of signal decreases as valinomycin increases (Table 3). In terms of biology this means that the potential difference between the far fields increases as the intracellular potential becomes more negative. So, these results confirm the hypothesis that by adding valinomycin we are able to change the potential in the vicinity of the membrane.

In order to evaluate data from the experiments, we add a linear approximation to all curves of Figures 6–10. From this approach, we get the slopes presented in table 3. By normalising these slopes for each solution by the slope of the control signal for the same buffer solution, we get Figure 11.

Because of different laboratory conditions during these experiments, we are unable to compare them directly. However, if we take a look at table 3, there are similarities, for example as soon as we add valinomycin the signal increases compare to the signal without valinomycin (sample 1 from table 3). Plus, the more valino-

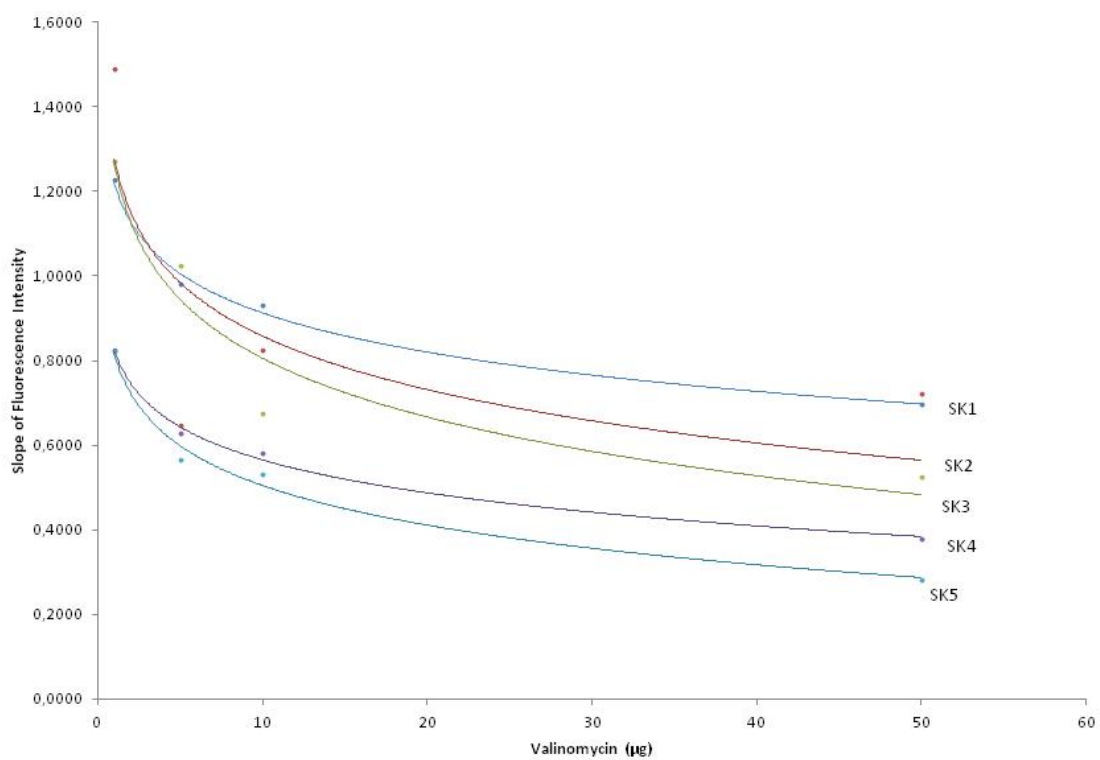


Figure 11: Normalised slopes from buffer solutions SK<sub>i</sub> versus amount of valinomycin in  $\mu\text{g}$ , where the dark blue line represents the data for solution SK<sub>1</sub>, the red line for SK<sub>2</sub>, the light green line for SK<sub>3</sub>, the purple line for SK<sub>4</sub> and the light blue line for SK<sub>5</sub>.

mycin we add, the less signal we obtain, which corresponds to literature findings where valinomycin allows potassium ions to freely cross the membrane out of the cell [4, 16, 27]. This motion does not allow the negatively charged dye molecules to diffuse so easily across the membrane, and thus we have less signal measured.

## 2.4 Conclusions

Our experiments have shown that the more valinomycin is added, the less amount of dye inserts the cell. As described in section 2.3, the addition of valinomycin decreases the intracellular concentration of potassium ions and the potential distribution inside the cell. The decrease of potassium distribution inside the cell in its turn decreases the crossing of charged molecules from outside to inside.

In quantifying the curves from Figures 6–10, we get the slopes for each curve that represents data. Figure 11 represents the slopes for each signal for valinomycin normalized by the slope for the control vs the amount of valinomycin added. From this figure we get an indirect way of quantifying the flux of potassium ions from the intracellular to the extracellular area, plus a way of quantifying the alterations of the potential inside the cell.

For example, an addition of 4  $\mu\text{g}$  more valinomycin (from 1 to 5  $\mu\text{g}$ ) in an environment of 100 mM of potassium results in a approximate 25% decrease of the signal value (values from table 3), which would mean a 25% drop in the distribution of the dye inside the cell. If the rest of the procedures, such as potassium–potential relationship and potential–dye relationship, are proportional then we should expect an alteration of order of 25% of the potential inside the cell (the potential becomes more negative) and a 25% increase in the efflux of potassium ions.

### 3 Modelling the electrostatic properties of a single cell as a response to pH changes

The following model is formulated based on an electrolyte consisted of sodium, potassium, hydrogen and chloride ions. Although during the experimental part we didn't take into consideration the effect of possible pH alterations, we decided to examine in the mathematical modelling if protons have an effect in the potential distribution near the membrane.

Our goal is to derive a simplified model of the electrochemical behavior near the cell membrane. In order to simplify the model, we assume that the membrane is planar, occupying the region  $|x^*| < \alpha^*$ , as illustrated in Figure 4.

Assuming one-dimensional distributions for the ion concentrations, e.g. when the flux of ions and the electric field are transverse to the membrane (Figure 4), and zero flux at steady state approach, we get the following equation for ionic concentration, from equation (1)

$$-D^\pm \left( \frac{dC^\pm}{dx^*} \pm \frac{F}{RT} C^\pm \frac{d\phi^*}{dx^*} \right) = 0 , \quad (8)$$

where  $x^*$  is the axis perpendicular to the membrane.

We take into consideration only sodium ( $Na$ ), potassium ( $K$ ), chloride ( $Cl$ ) and hydrogen ions ( $H$ ); the first three ions because of their high concentration in the electrolyte solution compared to other ions and hydrogen ions because of the potential link to pH ( $pH = -\log_{10} [H]$ ).

For every species we have a Nernst-Planck equation,

$$-D_{Na^+} \left( \frac{d[Na]}{dx^*} + \frac{F}{RT}[Na] \frac{d\phi^*}{dx^*} \right) = 0 , \quad (9)$$

$$-D_{K^+} \left( \frac{d[K]}{dx^*} + \frac{F}{RT}[K] \frac{d\phi^*}{dx^*} \right) = 0 , \quad (10)$$

$$-D_{H^+} \left( \frac{d[H]}{dx^*} + \frac{F}{RT}[H] \frac{d\phi^*}{dx^*} \right) = 0 , \quad (11)$$

$$-D_{Cl^-} \left( \frac{d[Cl]}{dx^*} - \frac{F}{RT}[Cl] \frac{d\phi^*}{dx^*} \right) = 0 . \quad (12)$$

The potential distribution is described by Poisson's equation

$$\begin{aligned} \frac{d}{dx^*} \left[ \varepsilon^*(x^*) \frac{d\phi^*}{dx^*} \right] &= -f_+^* \delta(x^* - \alpha^*) - f_-^* \delta(x^* + \alpha^*) \\ &+ F ([Cl] - [Na] - [K] - [H]) (1 + \mathcal{H}(x^* - \alpha^*) - \mathcal{H}(x^* + \alpha^*)) , \end{aligned} \quad (13)$$

where  $f_+^*, f_-^*$  stand for the surface charge density on the inner and outer membrane respectively,  $\varepsilon^*(x^*)$  for the electrical permittivity,  $\alpha^*$  is half the membrane's length (Figure 4) and  $\mathcal{H}(x^*)$  the Heaviside function.

The electric permittivity is non-uniform, being given by

$$\varepsilon^*(x^*) = \varepsilon_{\text{out}}^* \text{ if } |x^*| > \alpha^* , \quad (14)$$

$$\varepsilon^*(x^*) = \varepsilon_{\text{m}}^* \text{ if } |x^*| < \alpha^* , \quad (15)$$

where  $\varepsilon_{\text{out}}^*$  stands for the permittivity in the bulk solution and  $\varepsilon_{\text{m}}^*$  the permittivity in the membrane.

We now introduce conditions for the far fields. We assume that both the potential and the ionic concentrations reach a constant value. Moreover, there is electroneu-

trality at the far fields. In the intracellular area, as  $x^* \rightarrow \infty$ ,

$$\phi^* \rightarrow \phi_\infty^* , \quad (16)$$

$$[Na] \rightarrow [Na]_\infty , \quad (17)$$

$$[K] \rightarrow [K]_\infty , \quad (18)$$

$$[H] \rightarrow [H]_\infty , \quad (19)$$

$$[Cl] \rightarrow [Na]_\infty + [K]_\infty + [H]_\infty , \quad (20)$$

where  $\phi_\infty^*$  is the potential value when  $x^* \rightarrow \infty$ ,  $[Na]_\infty$  the concentration of sodium ions when  $x^* \rightarrow \infty$ ,  $[K]_\infty$  the concentration of potassium cations at the far field inside the cell and  $[H]_\infty$  the concentration of hydrogen ions when  $x^* \rightarrow \infty$ . In the extracellular area, as  $x^* \rightarrow -\infty$ ,

$$\phi^* \rightarrow \phi_{-\infty}^* , \quad (21)$$

$$[Na] \rightarrow [Na]_{-\infty} , \quad (22)$$

$$[K] \rightarrow [K]_{-\infty} , \quad (23)$$

$$[H] \rightarrow [H]_{-\infty} , \quad (24)$$

$$[Cl] \rightarrow [Na]_{-\infty} + [K]_{-\infty} + [H]_{-\infty} . \quad (25)$$

where  $\phi_{-\infty}^*$  the value for the far field potential,  $[Na]_{-\infty}$  the value for sodium cations concentration when  $x^* \rightarrow -\infty$ ,  $[K]_{-\infty}$  the concentration for potassium ions when  $x^* \rightarrow -\infty$ ,  $[H]_{-\infty}$  the concentration for hydrogen cations when  $x^* \rightarrow -\infty$ .

On either side of the membrane, we assume no jump in the potential. In other words,

$$\phi^*|_{x^*=\alpha^{*+}} = \phi^*|_{x^*=\alpha^{*-}} , \quad (26)$$

$$\phi^*|_{x^*=-\alpha^{*+}} = \phi^*|_{x^*=-\alpha^{*-}} . \quad (27)$$

Furthermore, we integrate equation (13) to relate the electric field to the surface charge density

$$\varepsilon_{\text{out}}^* \frac{d\phi^*}{dx^*} \Big|_{x^*=\alpha^{*+}} - \varepsilon_{\text{m}}^* \frac{d\phi^*}{dx^*} \Big|_{x^*=\alpha^{*-}} = -f_+^* , \quad (28)$$

$$\varepsilon_{\text{m}}^* \frac{d\phi^*}{dx^*} \Big|_{x^*=-\alpha^{*+}} - \varepsilon_{\text{out}}^* \frac{d\phi^*}{dx^*} \Big|_{x^*=-\alpha^{*-}} = -f_-^* . \quad (29)$$

According to the “Fluid Mosaic Model of the Membrane” [98], there are two different kinds of phospholipids for mammalian cells; negatively charged and neutral ones (uncharged). The charged phospholipids are responsible for the surface charge density of the membrane leaflets. At the same time, charged phospholipids are able to interact with hydrogen ions that are circulating free in the bulk area, creating a shielding effect for the membrane charge density.

The same equations and calculations apply for both membrane leaflets, so from now on, instead of using different notations we use  $\pm$  where  $+$  stands for the inner leaflet of the membrane and  $-$  for the outer leaflet of the membrane. We assume that there is a fixed quantity of phospholipids in each leaflet (meaning that phospholipids are neither destroyed nor produced). Then, in an attempt to simplify calculations, we assume that the rate of the reaction between protons (hydrogen ions) and charged molecules is proportional to the concentration of protons times the concentration of charged molecules. Plus, we assume that only hydrogen ions close enough to the membrane can take part in the reaction.

The reaction of phospholipids and hydrogen ions is chemically described as



a reaction that we assume to be in, where  $\text{PL}_{\pm}$  are the phospholipids that are negatively charged ( $-$ ) on the leaflets ( $\pm$ ),  $\text{H}^{\pm}$  the hydrogen ions near the leaflet and  $\text{PLH}_{\pm}$  the phospholipids already bound to hydrogen ions on the leaflet.  $k_f^*$  and  $k_b^*$  are the kinetic constants for the forward and the backward reaction respectively.

$\mathcal{N}_{\pm}^{\text{total}}$  is the number of phospholipids on the membrane.  $\mathcal{N}_{\pm}^{\text{NC}}$  is the number of non-charged phospholipids on the membrane.  $\mathcal{N}_{\pm}^{-}$  is the number of phospholipids that are negatively charged on the membrane.  $\mathcal{N}_{\pm}^{\text{H}}$  is the number of phospholipids of the membrane that were charged but have interacted with hydrogen ions. Assuming that the total number of phospholipids is conserved,

$$\mathcal{N}_{\pm}^{\text{total}} = \mathcal{N}_{\pm}^{\text{NC}} + \mathcal{N}_{\pm}^{-} + \mathcal{N}_{\pm}^{\text{H}}. \quad (31)$$

Taking into consideration that the surface concentration equals the number of molecules divided by the surface area, a different form of equation (31) concerning the conservation of phospholipids is

$$[\text{PL}_{\pm}^{\text{total}}] = [\text{PL}_{\pm}^{\text{NC}}] + [\text{PL}_{\pm}^{-}] + [\text{PLH}_{\pm}], \quad (32)$$

Let  $p_{\pm}$  be the fraction of charged phospholipids,

$$p_{\pm} = \frac{[\text{PL}_{\pm}^{-}]}{[\text{PL}_{\pm}^{\text{total}}]}, \quad (33)$$

and  $p_{H\pm}$  the fraction of phospholipids having already interacted with protons,

$$p_{H\pm} = \frac{[\text{PLH}_{\pm}]}{[\text{PL}_{\pm}^{\text{total}}]}. \quad (34)$$

The fraction of non-charged phospholipids is  $\beta_{\pm}$

$$\beta_{\pm} = \frac{\mathcal{N}_{\text{PL}_{\pm}^{\text{NC}}}}{\mathcal{N}_{\text{PL}_{\pm}^{\text{total}}}}, \quad (35)$$

which in terms of surface concentration is formulated as

$$[\text{PL}_{\pm}^{\text{NC}}] = \beta_{\pm} [\text{PL}_{\pm}^{\text{total}}]. \quad (36)$$

For the reaction (30), we assume first order kinetics, as mentioned earlier. This is mathematically translated into

$$\frac{d[\text{PLH}_{\pm}]}{dt} = k_f^* [\text{PL}_{\pm}^{-}] [H]_{x^*=\pm\alpha^*\pm} - k_b^* [\text{PLH}_{\pm}]. \quad (37)$$

Moreover, we assume steady state, so

$$\frac{d[\text{PLH}_{\pm}]}{dt} = 0, \quad (38)$$

which results in

$$[\text{PLH}_{\pm}] = k^* [\text{PL}_{\pm}^{-}] [H]_{x^*=\pm\alpha^*\pm}, \quad (39)$$

where

$$k^* = \frac{k_f^*}{k_b^*}. \quad (40)$$

The total concentration of phospholipids (equation 32) has now the following form

$$[\text{PL}_{\pm}^{\text{total}}] = \beta_{\pm} [\text{PL}_{\pm}^{\text{total}}] + p_{\pm} [\text{PL}_{\pm}^{\text{total}}] + p_{H\pm} [\text{PL}_{\pm}^{\text{total}}], \quad (41)$$

which is simplified to

$$1 = \beta_{\pm} + p_{\pm} + p_{H^{\pm}} . \quad (42)$$

By solving the equations (39), (41) and (42) we get

$$p_{\pm} = \frac{1 - \beta_{\pm}}{1 + k^* [H]_{x^* = \pm \alpha^*}} , \quad (43)$$

$$p_{H^{\pm}} = \frac{1 - \beta_{\pm}}{1 + k^* [H]_{x^* = \pm \alpha^*}} k^* [H]_{x^* = \pm \alpha^*} , \quad (44)$$

$$[\text{PL}_{\pm}^-] = \frac{1 - \beta_{\pm}}{1 + k^* [H]_{x^* = \pm \alpha^*}} [\text{PL}_{\pm}^{\text{total}}] , \quad (45)$$

$$[\text{PLH}_{\pm}] = \frac{1 - \beta_{\pm}}{1 + k^* [H]_{x^* = \pm \alpha^*}} k^* [H]_{x^* = \pm \alpha^*} [\text{PL}_{\pm}^{\text{total}}] , \quad (46)$$

$$[\text{PL}_{\pm}^{\text{total}}] = \beta_{\pm} [\text{PL}_{\pm}^{\text{total}}] . \quad (47)$$

The surface charge density is proportional to the concentration of charged phospholipids

$$f_{\pm}^* = Q N_{\text{Av}} [\text{PL}_{\pm}^-] , \quad (48)$$

and is otherwise expressed as

$$f_{\pm}^* = \psi_{\pm} f_{\pm} , \quad (49)$$

where

$$\psi_{\pm} = (1 - \beta_{\pm}) Q N_{\text{Av}} [\text{PL}_{\pm}^{\text{total}}] , \quad (50)$$

$$f_{\pm} = \frac{1}{1 + k^* [H]_{x^* = \pm \alpha^*}} . \quad (51)$$

### 3.1 Nondimensionalization

We non-dimensionalize the equations described in the previous section by scaling lengths on  $\alpha^*$ , the membrane half-length, and the potential on the thermal voltage  $RT/F$ , so that

$$x^* = \alpha^* x, \phi^* = \frac{RT}{F} \phi. \quad (52)$$

We also non-dimensionalize the ionic concentrations using the potassium concentration at the far field inside the cell ( $[K]_\infty$ ) for sodium, potassium and chloride ions and the hydrogen concentration at the far field ( $[H]_\infty$ ) for protons

$$[Na] = [K]_\infty N, [K] = [K]_\infty K, [Cl] = [K]_\infty C, [H] = [H]_\infty H. \quad (53)$$

Likewise we write

$$\varepsilon^*(x^*) = \varepsilon_{\text{out}}^* \varepsilon(x). \quad (54)$$

The dimensional equations for the concentrations (9)-(12) in  $|x| > 1$  become

$$\frac{dN}{dx} + N \frac{d\phi}{dx} = 0, \quad (55)$$

$$\frac{dK}{dx} + K \frac{d\phi}{dx} = 0, \quad (56)$$

$$\frac{dH}{dx} + H \frac{d\phi}{dx} = 0, \quad (57)$$

$$\frac{dC}{dx} - C \frac{d\phi}{dx} = 0. \quad (58)$$

The Poisson equation for the potential (13) becomes

$$\begin{aligned} \frac{d}{dx} \left[ \varepsilon(x) \frac{d\phi}{dx} \right] &= -\mu_+ f_+ \delta(x-1) - \mu_- f_- \delta(x+1) \\ &+ \mu (C - N - K) (1 + \mathcal{H}(x-1) - \mathcal{H}(x+1)) \end{aligned} \quad (59)$$

where

$$\mu_\pm = \frac{\psi_\pm \alpha^* F}{\varepsilon_{\text{out}} RT}, \quad \mu = \frac{\alpha^{*2} F^2}{\varepsilon_{\text{out}}^*} [K_\infty], \quad (60)$$

$$f_\pm = \frac{1}{1 + k_H H|_{x=\pm 1}}, \quad k_H = k^* [H_\infty]. \quad (61)$$

From table 4, it is obvious that  $[H]_\infty/[K_\infty] \ll 1$ . That is why there is no hydrogen contribution in equation (59).

The electric permittivity conditions are also changed into

$$\varepsilon(x) = 1 \text{ if } |x| > 1, \quad (62)$$

$$\varepsilon(x) = \varepsilon_m \text{ if } |x| < 1. \quad (63)$$

where  $\varepsilon_m = \varepsilon_m^*/\varepsilon_{out}^*$  is the dimensionless permittivity of the membrane.

Far inside the cell, the boundary conditions are

$$\phi \rightarrow \phi_\infty, \quad (64)$$

$$N \rightarrow N_\infty, \quad (65)$$

$$K \rightarrow 1, \quad (66)$$

$$H \rightarrow 1, \quad (67)$$

$$C \rightarrow N_\infty + 1, \quad (68)$$

where  $\phi_\infty = F\phi_\infty^*/RT$  and  $N_\infty = [Na]_\infty/[K]_\infty$ . Far outside the cell the conditions are

$$\phi \rightarrow \phi_{-\infty}, \quad (69)$$

$$N \rightarrow N_{-\infty}, \quad (70)$$

$$K \rightarrow K_{-\infty}, \quad (71)$$

$$H \rightarrow H_{-\infty}, \quad (72)$$

$$C \rightarrow N_{-\infty} + K_{-\infty}, \quad (73)$$

where  $\phi_{-\infty} = F\phi_{-\infty}^*/RT$ ,  $N_{-\infty} = [Na]_{-\infty}/[K]_\infty$ ,  $K_{-\infty} = [K]_{-\infty}/[K]_\infty$  and  $H_{-\infty} = [H]_{-\infty}/[H]_\infty$ .

On either side of the membrane, the jump conditions (26)–(29) in dimensionless form are

$$\phi_{x=1^+} = \phi_{x=1^-}, \quad (74)$$

$$\phi_{x=-1^+} = \phi_{x=-1^-}, \quad (75)$$

$$\frac{d\phi}{dx}\Big|_{x=1^+} - \varepsilon_m \frac{d\phi}{dx}\Big|_{x=1^-} = -\mu_+ f_+, \quad (76)$$

$$\varepsilon_m \frac{d\phi}{dx}\Big|_{x=-1^+} - \frac{d\phi}{dx}\Big|_{x=-1^-} = -\mu_- f_-. \quad (77)$$

### 3.2 Linearization

For a first approach to the non-linear solution of our system, we introduce a number of  $\tilde{\phantom{x}}$  parameters in order to linearize the equations governing the ion concentration in the bulk solutions at the steady state case.

$\Delta$  denotes a relatively small difference in the far field potentials

$$\Delta = \phi_{\infty} - \phi_{-\infty} . \quad (78)$$

The ionic concentrations are formulated based on far field concentrations and the  $\Delta$  parameter

$$N = N_{-\infty} + \Delta N_{-\infty} \tilde{N} , \quad (79)$$

$$K = K_{-\infty} + \Delta K_{-\infty} \tilde{K} , \quad (80)$$

$$H = H_{-\infty} + \Delta H_{-\infty} \tilde{H} , \quad (81)$$

$$C = (N_{-\infty} + K_{-\infty}) + \Delta (N_{-\infty} + K_{-\infty}) \tilde{C} . \quad (82)$$

The potential is linearized relative to the potential at the far field outside the cell

$$\phi = \phi_{-\infty} + \Delta \tilde{\phi} . \quad (83)$$

The surface charge density on both membrane sides follows the same approach

$$f_{\pm} = \Delta \tilde{f}_{\pm} . \quad (84)$$

Equations (55)-(58) are now

$$\frac{d\tilde{N}}{dx} + \frac{d\tilde{\phi}}{dx} = 0 , \quad (85)$$

$$\frac{d\tilde{K}}{dx} + \frac{d\tilde{\phi}}{dx} = 0 , \quad (86)$$

$$\frac{d\tilde{H}}{dx} + \frac{d\tilde{\phi}}{dx} = 0 , \quad (87)$$

$$\frac{d\tilde{C}}{dx} - \frac{d\tilde{\phi}}{dx} = 0 . \quad (88)$$

The equation (59) for the potential distribution is

$$\begin{aligned} \frac{d}{dx} \left[ \varepsilon(x) \frac{d\tilde{\phi}}{dx} \right] &= -\mu_+ \tilde{f}_+ \delta(x-1) - \mu_- \tilde{f}_- \delta(x+1) \\ &+ \mu \left[ (N_{-\infty} + K_{-\infty}) \tilde{C} - N_{-\infty} \tilde{N} - K_{-\infty} \tilde{K} \right] (1 + \mathcal{H}(x-1) - \mathcal{H}(x+1)) \end{aligned} \quad (89)$$

We also transform the boundary conditions for both the intracellular and the extracellular region. In detail, inside the cell,  $x \rightarrow \infty$ , (64)–(68) are

$$\tilde{\phi} \rightarrow 1, \quad (90)$$

$$\tilde{N} \rightarrow \frac{N_{\infty} - N_{-\infty}}{\Delta N_{-\infty}}, \quad (91)$$

$$\tilde{K} \rightarrow \frac{1 - K_{-\infty}}{\Delta K_{-\infty}}, \quad (92)$$

$$\tilde{H} \rightarrow \frac{1 - H_{-\infty}}{\Delta H_{-\infty}}, \quad (93)$$

$$\tilde{C} \rightarrow \frac{(N_{\infty} + 1) - (N_{-\infty} + K_{-\infty})}{\Delta(N_{-\infty} + K_{-\infty})}, \quad (94)$$

while as  $x \rightarrow -\infty$ , (69)–(73) turn into

$$\tilde{\phi} \rightarrow 0, \quad (95)$$

$$\tilde{N} \rightarrow 0, \quad (96)$$

$$\tilde{K} \rightarrow 0, \quad (97)$$

$$\tilde{H} \rightarrow 0, \quad (98)$$

$$\tilde{C} \rightarrow 0. \quad (99)$$

All the  $\tilde{\phantom{x}}$  have to be order unity in order for the linearisation to be appropriate.

The jump conditions (74)–(77) on either side of the membrane still hold as

$$\tilde{\phi}|_{x=1^+} = \tilde{\phi}|_{x=1^-}, \quad (100)$$

$$\tilde{\phi}|_{x=-1^+} = \tilde{\phi}|_{x=-1^-}, \quad (101)$$

$$\frac{d\tilde{\phi}}{dx}|_{x=1^+} - \varepsilon_m \frac{d\tilde{\phi}}{dx}|_{x=1^-} = -\mu_+ \tilde{f}_+, \quad (102)$$

$$\varepsilon_m \frac{d\tilde{\phi}}{dx}|_{x=-1^+} - \frac{d\tilde{\phi}}{dx}|_{x=-1^-} = -\mu_- \tilde{f}_-. \quad (103)$$

The general solution for the ionic equations (85)-(88) is given as

$$\tilde{N} = -\tilde{\phi} + c_1^\pm, \quad (104)$$

$$\tilde{K} = -\tilde{\phi} + c_2^\pm, \quad (105)$$

$$\tilde{H} = -\tilde{\phi} + c_3^\pm, \quad (106)$$

$$\tilde{C} = \tilde{\phi} + c_4^\pm, \quad (107)$$

where  $c_1^\pm, c_2^\pm, c_3^\pm, c_4^\pm$  are constants,

For the intracellular area, the constants are

$$c_1^+ = \frac{N_\infty + (\Delta - 1) N_{-\infty}}{\Delta N_{-\infty}}, \quad (108)$$

$$c_2^+ = \frac{1 + (\Delta - 1) K_{-\infty}}{\Delta K_{-\infty}}, \quad (109)$$

$$c_3^+ = \frac{1 + (\Delta - 1) H_{-\infty}}{\Delta H_{-\infty}}, \quad (110)$$

$$c_4^+ = \frac{(N_\infty + 1) - (\Delta + 1)(N_{-\infty} + K_{-\infty})}{\Delta(N_{-\infty} + K_{-\infty})}, \quad (111)$$

while outside of the cell, they all equal to zero,

$$c_1^- = 0, c_2^- = 0, c_3^- = 0, c_4^- = 0. \quad (112)$$

We then solve (89) for the potential distribution, using conditions (90) and (95) for the potential in the far fields, which results in the following equations

$$\tilde{\phi} = A \exp \left[ -x \sqrt{2\mu(N_{-\infty} + K_{-\infty})} \right] + 1 \text{ when } x > 1, \quad (113)$$

$$\tilde{\phi} = Bx + D \text{ when } |x| < 1, \quad (114)$$

$$\tilde{\phi} = E \exp \left[ x \sqrt{2\mu(N_{-\infty} + K_{-\infty})} \right] \text{ when } x < -1. \quad (115)$$

Taking into consideration the jump conditions (100)–(103), we get the values for  $A, B, D, E$  parameters

$$A = \frac{1}{2} \left[ \frac{\mu_+ \tilde{f}_+ - \mu_- \tilde{f}_- + \sqrt{2\mu(N_{-\infty} + K_{-\infty})}}{\varepsilon_m + \sqrt{2\mu(N_{-\infty} + K_{-\infty})}} + \frac{\mu_+ \tilde{f}_+ + \mu_- \tilde{f}_-}{\sqrt{2\mu(N_{-\infty} + K_{-\infty})}} - 1 \right] \exp \left[ \sqrt{2\mu(N_{-\infty} + K_{-\infty})} \right], \quad (116)$$

Parameters	Values and Dimensions	Bibliography
$[K]_{\infty}$	140 mM	[1]
$[Na]_{\infty}$	5 mM	[1]
$[H]_{\infty}$	$10^{-7.2}$ M	[83]
$[K]_{-\infty}$	5 mM	[1]
$[Na]_{-\infty}$	140 mM	[1]
$[H]_{-\infty}$	$10^{-7.4}$ M	[83]
$\varepsilon_{\text{out}}^*$	$10^{-10}$ A*s/V*m	[69]
$\varepsilon_{\text{in}}^*$	$10^{-10}$ A*s/V*m	[69]
$\varepsilon_{\text{m}}^*$	$0.025 \cdot 10^{-10}$ A*s/V*m	[70]
$\beta_{\pm}$	0.7	[90]
$[PL_{\pm}^{\text{total}}]$	$10^{-5}$ mol/m <sup>2</sup>	[90]
$R$	8.314 J/mol*K	[69]
$F$	$9.65 \cdot 10^4$ J/mol*K	[69]
$T$	310 K	[69]
$\alpha^*$	5 nm	[90]
$Q$	$-1.6 \cdot 10^{-19}$ C/atom	[69]
$N_{\text{Av}}$	$6.023 \cdot 10^{23}$ atoms/mol	[69]
$k^*$	6.5	[74]

Table 4: Dimensional Parameters. Note that  $k^*$  is assumed to be order  $k_{Ac}$  which is the value for ATP energy requirement, the unit for all energy requirements at the cellular level [74].

$$B = \frac{\mu_+ \tilde{f}_+ - \mu_- \tilde{f}_- + \sqrt{2\mu(N_{-\infty} + K_{-\infty})}}{2 \left[ \sqrt{2\mu(N_{-\infty} + K_{-\infty})} + \varepsilon_{\text{m}} \right]}, \quad (117)$$

$$D = \frac{1}{2} \left[ \frac{\mu_+ \tilde{f}_+ + \mu_- \tilde{f}_-}{\sqrt{2\mu(N_{-\infty} + K_{-\infty})}} \right] + 1, \quad (118)$$

$$E = -\frac{1}{2} \left[ \frac{\mu_+ \tilde{f}_+ + \sqrt{2\mu(N_{-\infty} + K_{-\infty})}}{\varepsilon_{\text{m}}} - \frac{\mu_+ \tilde{f}_+ + \mu_- \tilde{f}_-}{\sqrt{2\mu(N_{-\infty} + K_{-\infty})}} - 1 \right] \exp \left[ \sqrt{2\mu(N_{-\infty} + K_{-\infty})} \right]. \quad (119)$$

We then plot the potential distribution throughout the cell versus the  $x$ -axis (Figure 12) and the ionic distribution (Figure 13). We are using parameters of table

Dimensionless Parameters	Values
$N_\infty$	0.99
$K_\infty$	1
$H_\infty$	1
$N_{-\infty}$	1
$K_{-\infty}$	0.98
$H_{-\infty}$	0.99
$\varepsilon_{\text{out}}$	1
$\varepsilon_{\text{m}}$	0.025
$\beta_{\pm}$	0.7
$f_{\pm}$	0.001
$\phi_\infty$	0.01
$\phi_{-\infty}$	0
$k_H$	$6.5 * 10^{-8}$

Table 5: Dimensionless parameters used for linearization. These parameters are calculated to be consistent with the linearization assumption.

5.

### 3.3 Non linear solutions

Because in nature, the concentration of ions differ from inside to outside of the cell, the linearized approach is not accurate enough when we want to calculate the potential distribution accurately. For that, we proceed in solving equations (55)–(58) explicitly. In order to determine the equation for the distribution of electric potential across the membrane,  $\phi(x)$ , and the distribution of sodium, potassium, hydrogen and chloride ions,  $N(x)$ ,  $K(x)$ ,  $H(x)$ ,  $C(x)$  respectively, we solve (55)

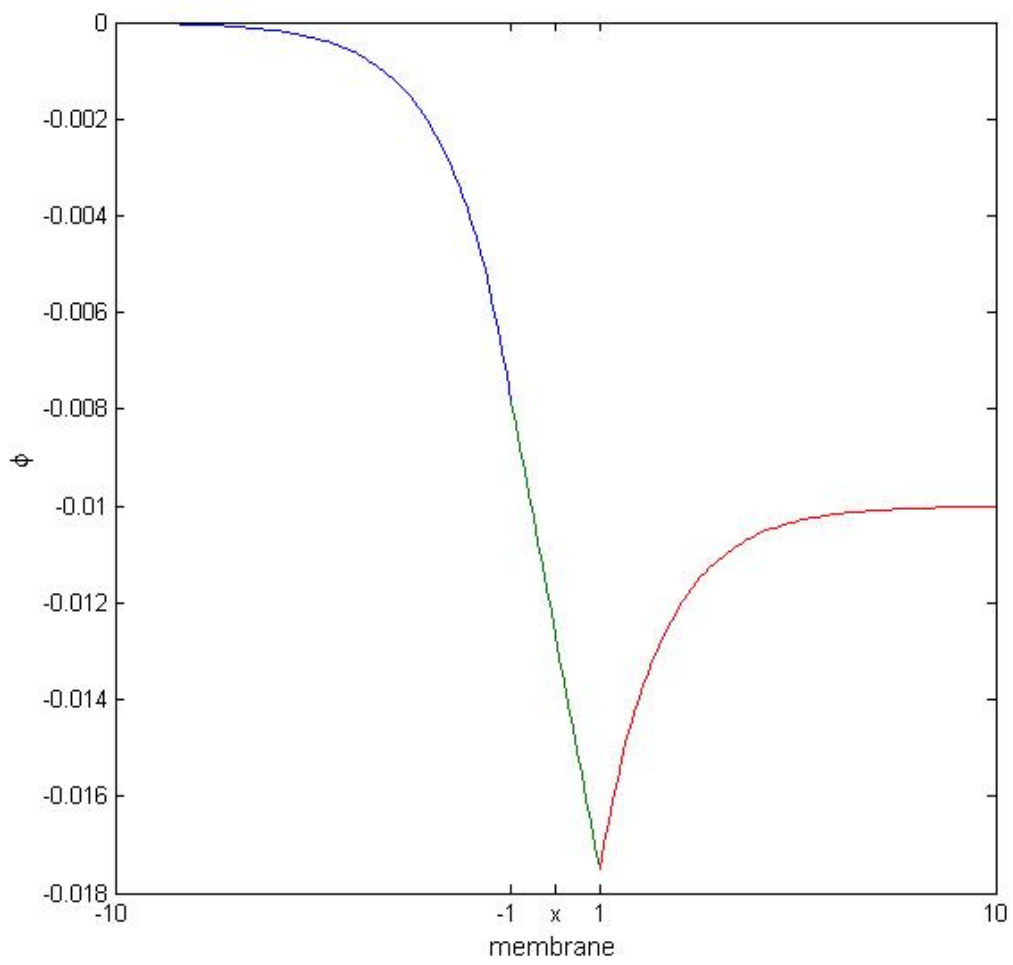


Figure 12: Linearized potential using values from table 5.

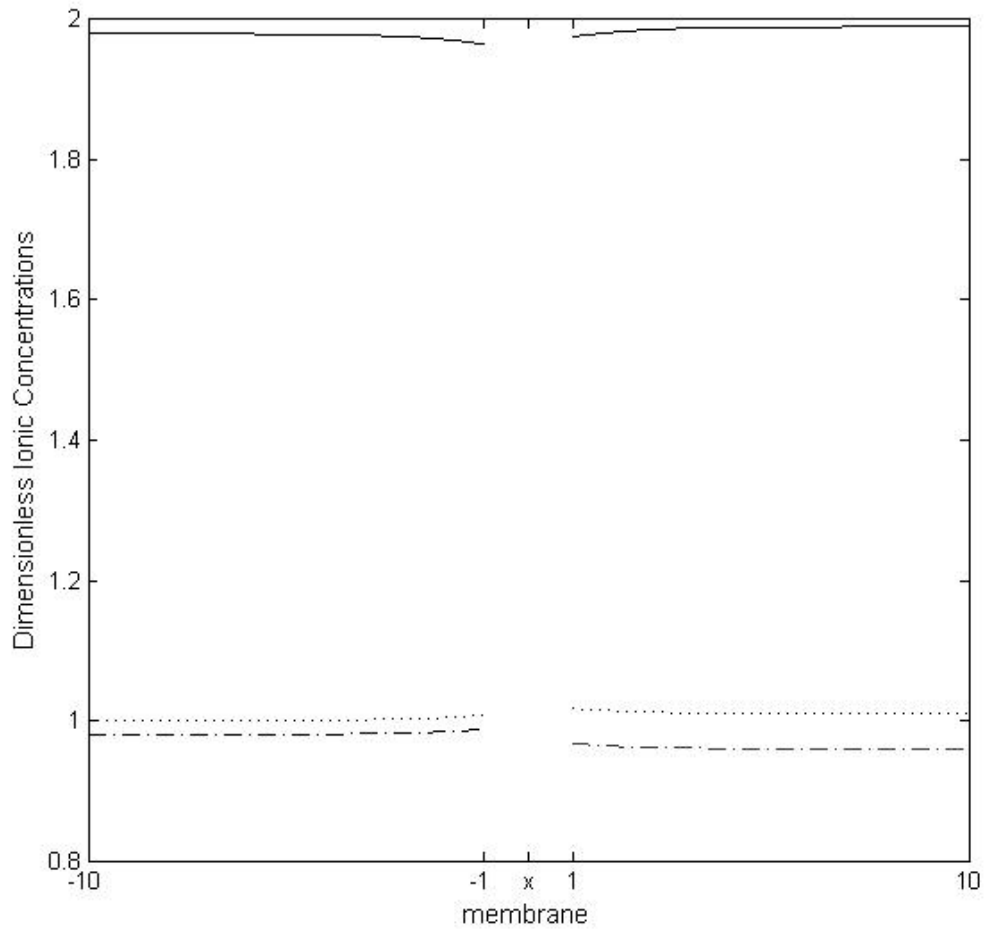


Figure 13: Linearized ionic concentrations using values from table 5, where the black solid lines represent the chloride distribution, the black dotted lines the sodium, the black dashed–dotted lines the potassium and the red dashed–dotted lines the hydrogen.

to (58) to obtain, when  $|x| > 1$ ,

$$N(x) = \exp(-\phi(x) + c_1^\pm), \quad (120)$$

$$K(x) = \exp(-\phi(x) + c_2^\pm), \quad (121)$$

$$H(x) = \exp(-\phi(x) + c_3^\pm), \quad (122)$$

$$C(x) = \exp(\phi(x) + c_4^\pm). \quad (123)$$

Applying the boundary conditions gives

$$N = N_{\pm\infty} \exp(-\phi + \phi_{\pm\infty}), \quad (124)$$

$$K = K_{\pm\infty} \exp(-\phi + \phi_{\pm\infty}), \quad (125)$$

$$H = H_{\pm\infty} \exp(-\phi + \phi_{\pm\infty}), \quad (126)$$

$$C = (N_{\pm\infty} + K_{\pm\infty}) \exp(\phi - \phi_{\pm\infty}), \quad (127)$$

while the expression for the electric potential is given by

$$\frac{d}{dx} \left( \frac{d\phi}{dx} \right) = \mu (C - N - K). \quad (128)$$

Introducing (120)–(123) gives

$$\frac{d^2\phi}{dx^2} = \mu (N_{\pm\infty} + K_{\pm\infty}) [\exp(\phi - \phi_{\pm\infty}) - \exp(-\phi + \phi_{\pm\infty})]. \quad (129)$$

By multiplying with  $\frac{d\phi}{dx}$

$$\frac{d\phi}{dx} \frac{d^2\phi}{dx^2} = \mu (N_{\pm\infty} + K_{\pm\infty}) [\exp(\phi - \phi_{\pm\infty}) - \exp(-\phi + \phi_{\pm\infty})] \frac{d\phi}{dx}, \quad (130)$$

which can be viewed also as

$$\frac{d}{dx} \left[ \frac{1}{2} \left( \frac{d\phi}{dx} \right)^2 \right] = \mu (N_{\pm\infty} + K_{\pm\infty}) \frac{d}{dx} [\exp(\phi - \phi_{\pm\infty}) + \exp(-\phi + \phi_{\pm\infty})]. \quad (131)$$

By integrating and stating  $F$  as the integration constant, we get

$$\frac{1}{2} \left( \frac{d\phi}{dx} \right)^2 = \mu (N_{\pm\infty} + K_{\pm\infty}) [\exp(\phi - \phi_{\pm\infty}) + \exp(-\phi + \phi_{\pm\infty})] + F. \quad (132)$$

Because of boundary conditions ( $\phi \rightarrow \phi_{\pm\infty}$ ), we calculate  $F$  as

$$F = -2\mu (N_{\pm\infty} + K_{\pm\infty}). \quad (133)$$

So, we have

$$\frac{1}{2} \left( \frac{d\phi}{dx} \right)^2 = \mu (N_{\pm\infty} + K_{\pm\infty}) [\exp(\phi - \phi_{\pm\infty}) + \exp(-\phi + \phi_{\pm\infty})] - 2\mu (N_{\pm\infty} + K_{\pm\infty}) , \quad (134)$$

which is simplified to

$$\frac{1}{2} \left( \frac{d\phi}{dx} \right)^2 = \mu (N_{\pm\infty} + K_{\pm\infty}) \left[ \exp\left(\frac{\phi - \phi_{\pm\infty}}{2}\right) - \exp\left(\frac{-\phi + \phi_{\pm\infty}}{2}\right) \right]^2 . \quad (135)$$

Thus

$$\frac{1}{\sqrt{2}} \frac{d\phi}{dx} = \pm \sqrt{\mu (N_{\pm\infty} + K_{\pm\infty})} \left[ \exp\left(\frac{\phi - \phi_{\pm\infty}}{2}\right) - \exp\left(\frac{-\phi + \phi_{\pm\infty}}{2}\right) \right] , \quad (136)$$

i.e.

$$\frac{d\phi}{dx} = \pm 2\sqrt{2\mu (N_{\pm\infty} + K_{\pm\infty})} \sinh\left(\frac{\phi - \phi_{\pm\infty}}{2}\right) , \quad (137)$$

which can be changed into

$$\frac{d\phi}{dx} = \pm 4\sqrt{2\mu (N_{\pm\infty} + K_{\pm\infty})} \frac{\tanh\left(\frac{\phi - \phi_{\pm\infty}}{4}\right)}{\operatorname{sech}^2\left(\frac{\phi - \phi_{\pm\infty}}{4}\right)} . \quad (138)$$

Separating variables results in

$$\int \frac{\operatorname{sech}^2\left(\frac{\phi - \phi_{\pm\infty}}{4}\right)}{\tanh\left(\frac{\phi - \phi_{\pm\infty}}{4}\right)} d\phi = \pm 4 \int \sqrt{2\mu (N_{\pm\infty} + K_{\pm\infty})} dx + \text{Constant} , \quad (139)$$

which leads to the solution

$$\phi = \phi_{\pm\infty} + 4 \tanh^{-1} \exp \left[ \pm \sqrt{2\mu (N_{\pm\infty} + K_{\pm\infty})} x + G_{\pm} \right] . \quad (140)$$

From the boundary conditions, we can determine the sign of the term within the exponential, giving

$$\phi = \phi_{\pm\infty} + 4 \tanh^{-1} \exp \left[ \mp x \sqrt{2\mu (N_{\pm\infty} K_{\pm\infty})} + G_{\pm} \right] . \quad (141)$$

In the meantime, we have to take into account the potential distribution within the membrane,  $|x| < 1$  ,

$$\frac{d^2\phi}{dx^2} = 0 , \quad (142)$$

so that

$$\phi = ux + w \tag{143}$$

where  $u$ ,  $w$  are integration constants.

We still have the jump conditions which will help us to determine integration constants  $G_{\pm}$ ,  $u$ ,  $w$ . However, this system cannot be solved analytically because of its complexity. Numerical solutions are shown in figure 14. Using the same parameters as in the linearized form of the model (figure 12), we get the same shape for the potential distribution across the membrane. The only difference lies in the potential values near the outer leaflet of the membrane. This is because the relation between repulsion and attraction forces is more complicated.

### 3.4 Results of electrostatic modelling

First of all, from equation (61) we see that as hydrogen concentration increases, the surface charge density decreases. However, from table 5,  $k_H$  is much smaller than unity, while  $H_{\pm 1}$  is order unity, so the term  $k_H H|_{x=\pm 1}$  is smaller than unity. As a result, the surface charge density is not affected by proton alterations. So, we have shown that the pH has a negligible effect on the surface charge density. From equation (59) the potential will remain constant no matter the increase or the decrease in hydrogen ion concentration.

Then we have described the potential distribution within our are of interest, which includes the cell and the surrounding electrolyte solution. We have two different forms:

- a linearized potential, based on analytical approximations and calculations, and
- a non-linear potential, based on numerical solutions.

Using the potassium concentrations from the experiments (Chapter 2) combined

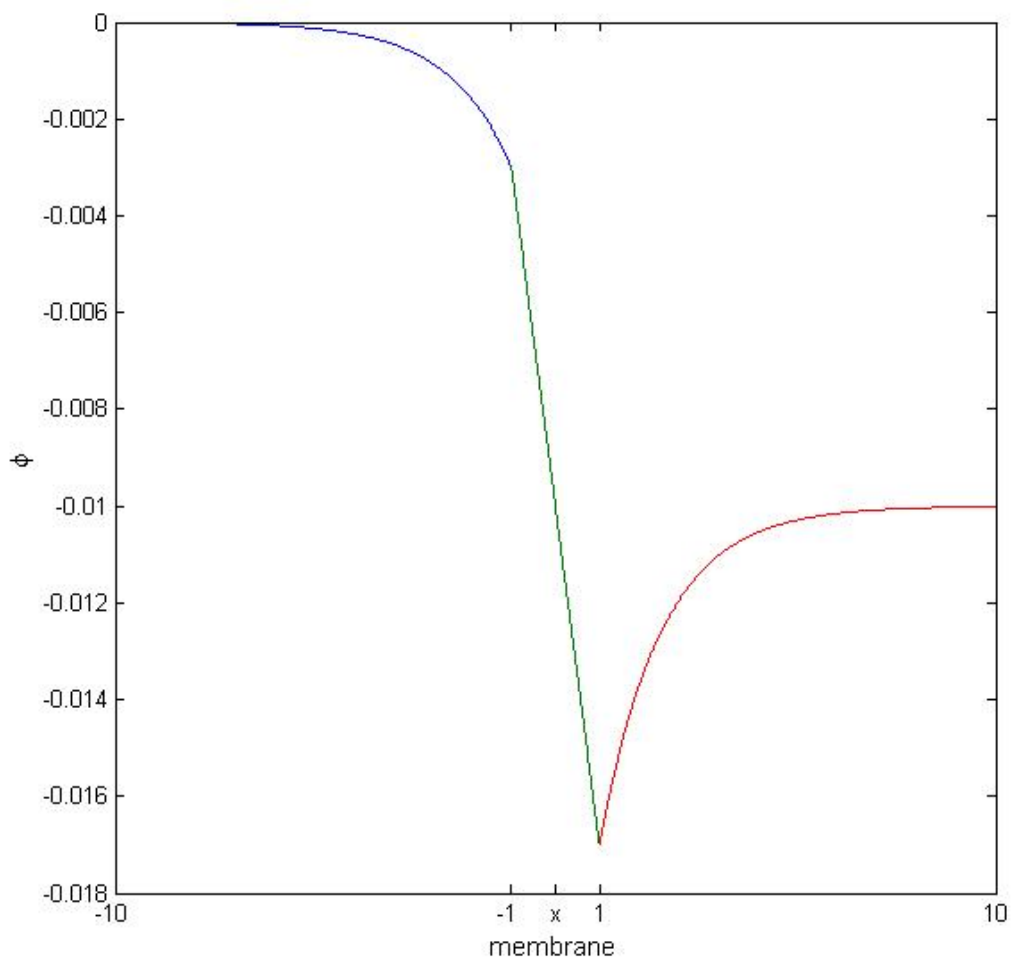


Figure 14: Non-linear potential distribution with the values from table 5.

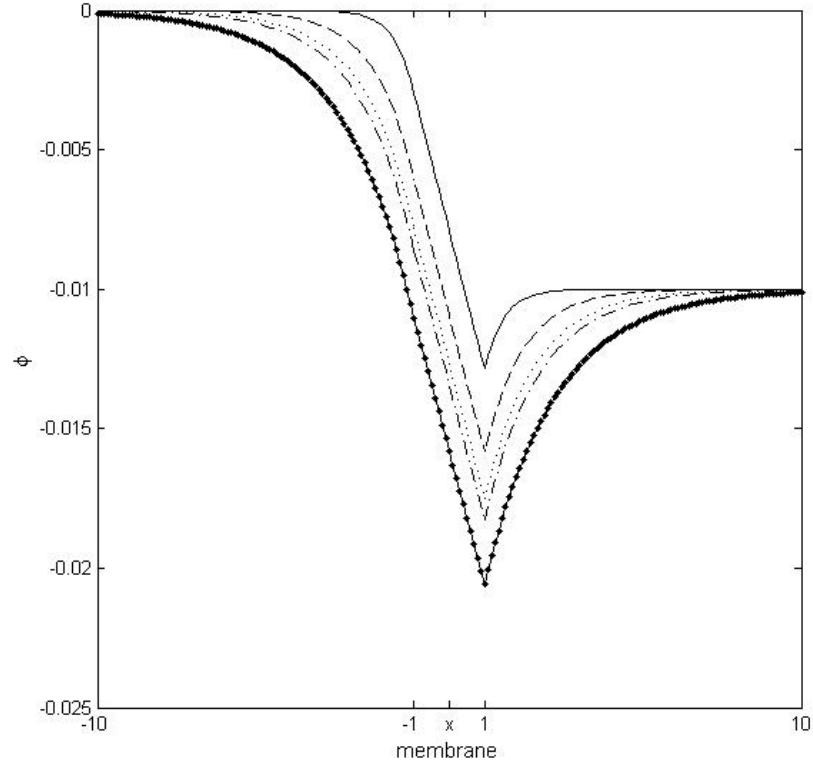


Figure 15: Linearised potential distribution when the extracellular potassium concentration ranges from 4.5mM to 164.5 mM, from table 1, and using parameters from table 5.

with the equations for the linearized potential distribution (equations 113–119) as a simple approach, we get the following five graphs for the potential distribution

In figure 15 the far field values are kept constant, while the potential distribution within the membrane preserves the same shape but different values. In detail, the more potassium we add in the extracellular environment, the potential reaches a more negative value within the membrane. When using potassium concentration different than the one found in nature (table 4), the ratio between the two dominant cations (sodium and potassium) is changed. As the total amount of potassium increases the ratio of sodium versus potassium decreases, so the potential well is getting deeper, because there are fewer cations surrounding the membrane. This is consistent with figure 12 if one knows that the signal intensity is proportional to the dye distribution within the cell. In other words, the transport of the dye across

the membrane depends on the potential distribution within the well which in turn depends on the extracellular potassium concentration. The larger the gap between the potential outside the membrane and the potential within the membrane will allow more dye molecules to cross the outer layer of the membrane.

## 4 Modelling the experimental results

In this chapter, we aim to combine the experimental results (chapter 2) with the modelling description (chapter 3). In section 4.1, we use a model for describing the valinomycin mechanism and its effect in the experimental procedure. In section 4.2, using Fokker–Planck approach, we determine the distribution of the probability density of the dye, near the cellular membrane. This distribution serves as an indirect evaluation of the signal exhibit by the dye when it fluorescents.

### 4.1 Valinomycin modelling

To describe the transport of valinomycin across the membrane we adapt the glucose–transporter model[39] by assuming that valinomycin follows a basic transport model

$$\frac{d[VK_i]}{dt} = k[VK_e] - k[VK_i] + k_+[K_i][V_i] - k_-[VK_i] , \quad (144)$$

$$\frac{d[VK_e]}{dt} = k[VK_i] - k[VK_e] + k_+[K_e][V_e] - k_-[VK_e] , \quad (145)$$

$$\frac{d[V_i]}{dt} = k[V_e] - k[V_i] + k_-[VK_i] - k_+[K_i][V_i] , \quad (146)$$

$$\frac{d[V_e]}{dt} = k[V_i] - k[V_e] + k_+[VK_e] - k_+[K_e][V_e] , \quad (147)$$

where  $VK_i$  stands for the potassium-valinomycin complex on the inner leaflet of the membrane,  $VK_e$  for the potassium-valinomycin complex on the outer leaflet of the membrane,  $K_i$  for the potassium ions inside the cell,  $K_e$  for the potassium ions outside the cell,  $V_i$  for free valinomycin on the inner leaflet of the membrane and  $V_e$  for free valinomycin on the outer leaflet of the membrane. Note that the membrane is assumed to consist of two phospholipic parts (figure 1), also know as leaflets. In figure 16, the upper straight line represents the outer leaflet of the membrane, while the lower straight line is the inner leaflet.  $[ ]$  represents the concentration of the substance within the brackets. Note that the concentration is per unit area when we are referring to valinomycin either free or bound to potassium while the concentration of potassium is per unit volume.  $k$  is the transport rate of valinomycin molecules

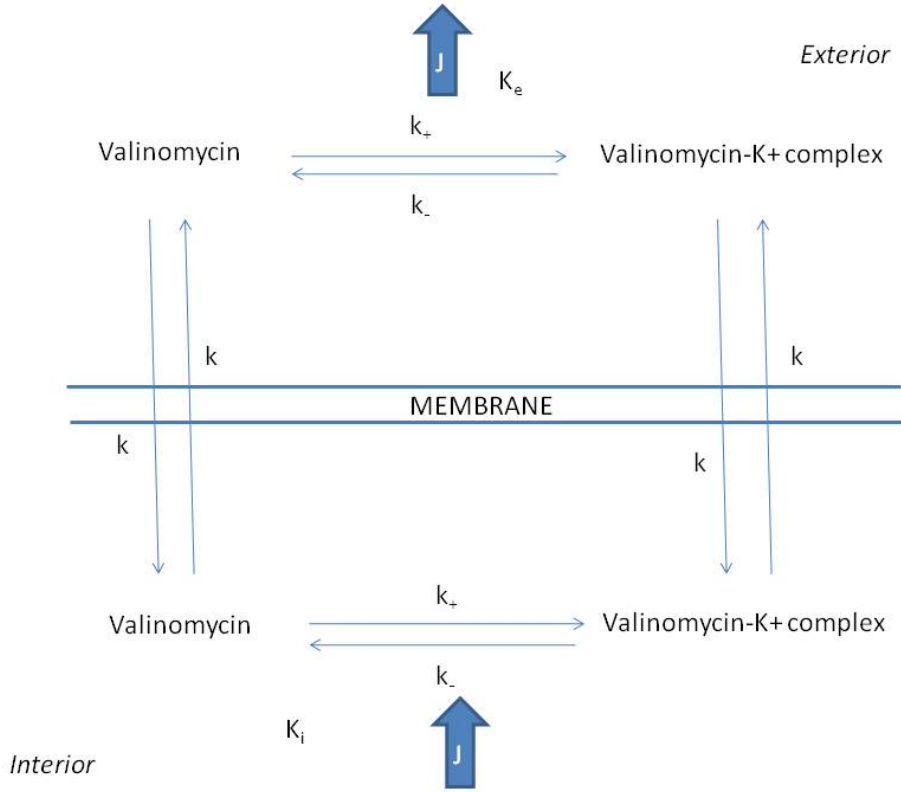


Figure 16: Schematic model of how valinomycin crosses the membrane

across the membrane,  $k_+$  is the association rate constant and  $k_-$  is the dissociation rate constant of the following reaction that forms the potassium–valinomycin complex



Valinomycin remains bound to the membrane at all times whereas free potassium ions are located in the bulk solution close to the membrane. According to [100],  $k = 2 \times 10^4 \text{ s}^{-1}$ ,  $k_+ = 5 \times 10^4 \text{ s}^{-1}$  and  $k_- = 5 \times 10^5 \text{ M}^{-1}\text{s}^{-1}$ .

The law of mass conservation applies for valinomycin, so equations (144)–(147) satisfy the following equation as well

$$[VK_e] + [VK_i] + [V_e] + [V_i] = [V_{total}] \quad (149)$$

where  $[V_{total}]$  is the total amount of valinomycin concentration either in a complex or in a free form, both on the inner and the outer leaflet of the membrane.

Parameters	Values and Dimensions	Source
$k$	$2 \times 10^4 \text{s}^{-1}$	[100]
$k_-$	$5 \times 10^4 \text{s}^{-1}$	[100]
$k_+$	$5 \times 10^5 \text{M}^{-1} \text{s}^{-1}$	[100]
$[V_{total}] (\times 10^{18} \text{mol/cell})$	8.99, 44.99, 89.9, 449.9	Experiments
$[K_i]_0$	140 mM	[1]
$[K_e] (\text{mM})$	4.5, 12, 50, 100, 164.5	Experiments
$r_{cell}$	$7.5 \times 10^{-6} \text{m}$	[32]
$V_{cell}$	$1.77 \times 10^{-15} \text{m}^3$	Volume of a sphere with radius $r_{cell}$

Table 6: Dimensional Parameters

The flux of molecules across the membrane is composed of a component from the outside to the transporter

$$J_{\text{on}} = k_+[K_e][V_e] - k_-[VK_e] \quad (150)$$

and a component from the transporter to inside the cell

$$J_{\text{off}} = k_-[VK_i] - k_+[K_i][V_i] . \quad (151)$$

In the steady state case, the flux from the transporter to inside the cell equals the flux outside to the transporter ( $J_{\text{on}} = J_{\text{off}} = J$ )

$$J = k_-[VK_i] - k_+[K_i][V_i] = k_+[K_e][V_e] - k_-[VK_e] . \quad (152)$$

The system of equations (144)–(147) has five unknown parameters, so a fifth equation is needed to fully solve the system. A conservation equation for potassium ions is required. While the extracellular potassium concentration remains constant, the concentration of potassium ions inside the cell is driven by the flux

$$\frac{d[K_i]V_{cell}}{dt} = JS_{cell} , \quad (153)$$

where  $V_{cell}$  is the cell volume and  $S_{cell}$  is the membrane surface area.

At  $t = 0$  , we assume that all valinomycin is located on the outer leaflet of the membrane  $[V_e]_0 = [V_{total}]$  ,  $[V_i]_0 = 0$  ,  $[VK_e]_0 = 0$  ,  $[VK_i]_0 = 0$  . The cytosolic

Parameters	Values	Equation
$K$	0.1	$K = k_-/k_+$
$\kappa$	0.4	$\kappa = K_d/K$
$K_e$	0.045, 0.12, 0.5, 1, 1.645	$K_e = [K_e]/K$
$\lambda$	$0.001[V_{total}]$	Table 6

Table 7: Dimensionless parameters for the cycle of valinomycin

potassium concentration is 140 mM, a typical value for mammalian cell lines. The extracellular potassium concentration varies as shown in table 6.

We now solve the system of equations (144)–(147) plus equation (153). In order to nondimensionalise and solve this system, we introduce the parameters  $K = \frac{k_-}{k_+}$ . We also introduce the nondimensional parameters  $VK_i = \frac{[VK_i]}{[V_{total}]}$ ,  $VK_e = \frac{[VK_e]}{[V_{total}]}$ ,  $V_i = \frac{[V_i]}{[V_{total}]}$ ,  $V_e = \frac{[V_e]}{[V_{total}]}$ ,  $K_i = \frac{[K_i]}{K}$ ,  $K_e = \frac{[K_e]}{K}$ ,  $\kappa = \frac{k}{k_-}$  and  $t = \frac{\tau}{k}$ . The variable for the non-dimensionalisation of time is the time needed for a molecule of valinomycin to cross the membrane.

The nondimensionalised system of equations is

$$\frac{dVK_i}{d\tau} = (VK_e - VK_i) + \frac{1}{\kappa} (K_i V_i - VK_i) , \quad (154)$$

$$\frac{dVK_e}{d\tau} = (VK_i - VK_e) + \frac{1}{\kappa} (K_e V_e - VK_e) , \quad (155)$$

$$\frac{dV_i}{d\tau} = (V_e - V_i) + \frac{1}{\kappa} (VK_i - K_i V_i) , \quad (156)$$

$$\frac{dV_e}{d\tau} = (V_i - V_e) + \frac{1}{\kappa} (VK_e - K_e V_e) , \quad (157)$$

$$\frac{dK_i}{d\tau} = \lambda (VK_i - K_i V_i) , \quad (158)$$

where  $\lambda = \frac{k_+ S_{cell}}{k V_{cell}} [V_{total}]$ , with the initial conditions  $V_{e_0} = 1$ ,  $V_{i_0} = 0$ ,  $VK_{e_0} = 0$ ,  $VK_{i_0} = 0$ ,  $K_{i_0} = 1.4$ . The rest of the dimensionless parameters are cited in table 7.

As shown from the figure 17 the different forms of valinomycin quickly reach a plateau for the concentrations. The time needed is approximately 0.05 seconds. Then a dynamic equilibrium is established where the concentration of each form

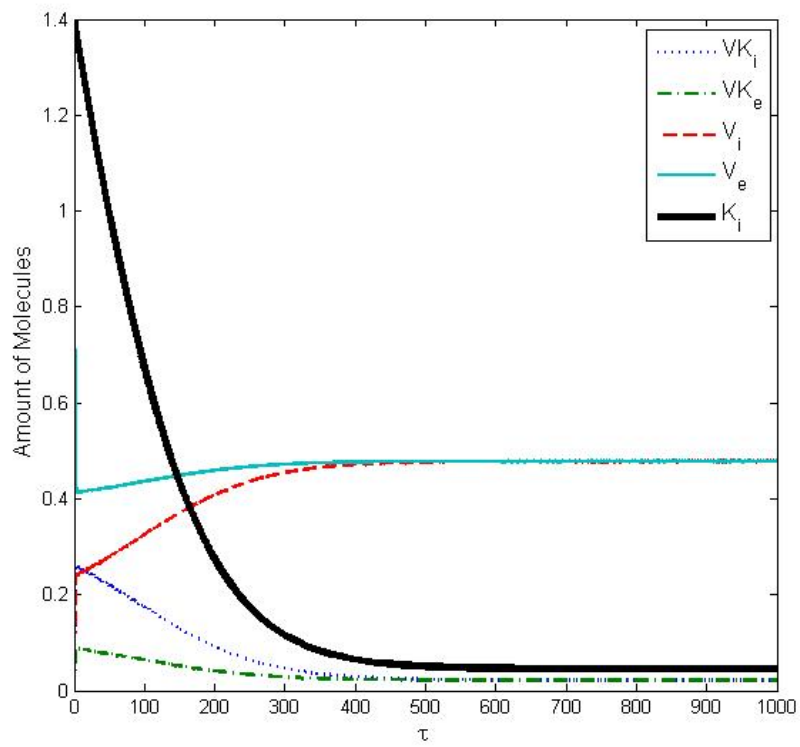


Figure 17: Schematic model of how valinomycin crosses the membrane, when we add 1 *μ*M valinomycin and 4.5 mM of potassium in the extracellular area.

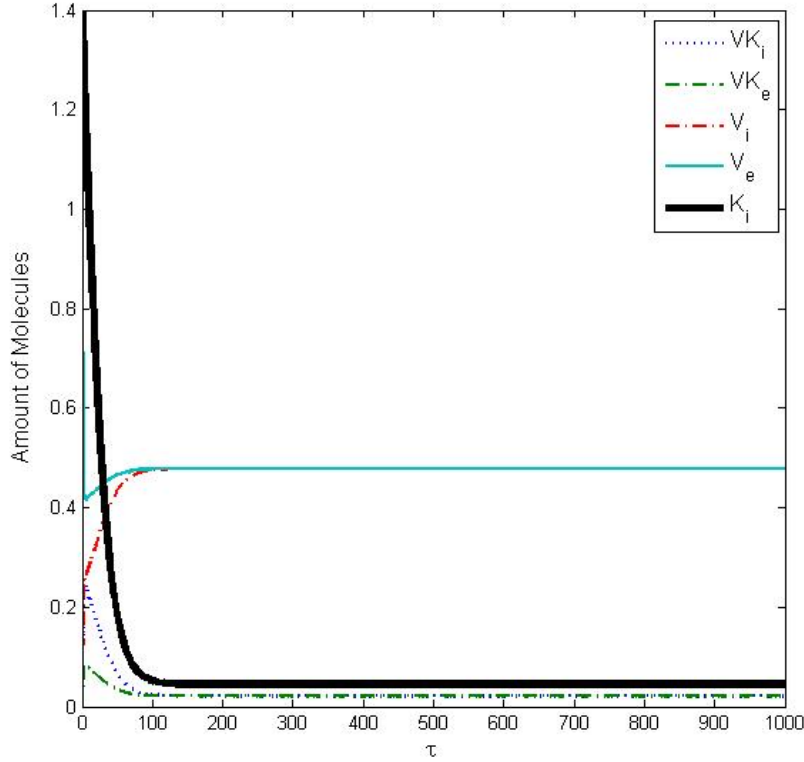


Figure 18: Schematic model of how valinomycin crosses the membrane, when we add 5  $\mu\text{g}$  valinomycin and 4.5 mM of potassium in the extracellular area.

remain the same, but there is still conversion from one form to the other.

We present here figures 18–20 where the only difference is the amount of valinomycin added, while the extracellular potassium concentration remains the same. The difference lies in the time needed for the system to reach equilibrium. In detail, the more valinomycin we add, the less time is needed for the plateau to occur.

## 4.2 Potential modelling

As stated in section 1.4, we use the Fokker–Planck equation (equation 7) to describe the probability of a particle being situated in a given position  $x$  at a certain time  $t$  when the particle moves under the influence of a force. In our case, we have a  $x$ -dependent electrostatic force, created by the distribution of potential at the cellular

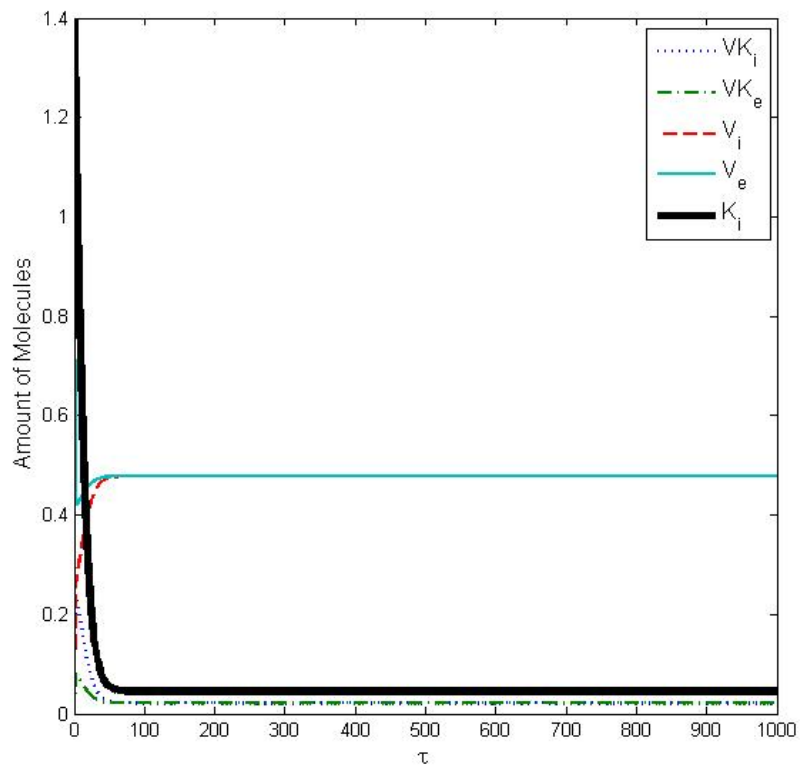


Figure 19: Schematic model of how valinomycin crosses the membrane, when we add 10  $\mu g$  valinomycin and 4.5 mM of potassium in the extracellular area.

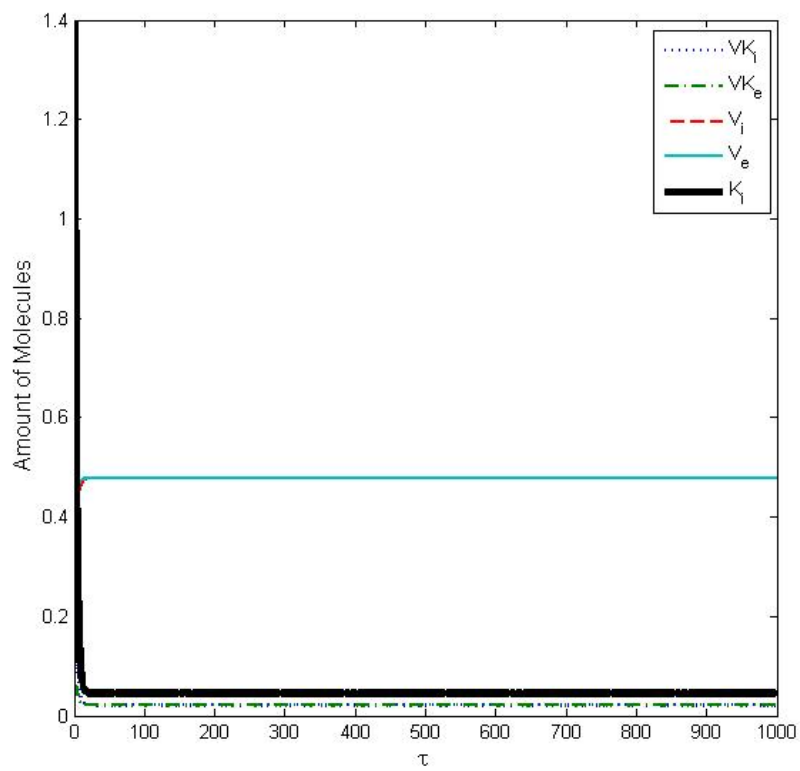


Figure 20: Schematic model of how valinomycin crosses the membrane, when we add 50  $\mu g$  valinomycin and 4.5 mM of potassium in the extracellular area.

level,

$$F(x^*) = -q \frac{d\phi^*}{dx^*} . \quad (159)$$

Note that  $\phi^*$  stands for the dimensional potential. We have calculated the dimensionless potential distribution in Chapter 3. Using the previous notations for non-dimensionalization (section 3.1) for the variables and introducing

$$t = t^* \tau , \quad (160)$$

as the time needed for the dye to cross the membrane, the Fokker–Planck equation has the following dimensionless form

$$\frac{\partial P}{\partial \tau} = \frac{qRTt^*}{a^{*2}FM\gamma} \frac{\partial}{\partial x} \left[ \frac{d\phi}{dx} P \right] + \frac{Dt^*}{\alpha^{*2}} \frac{\partial^2 P}{\partial x^2} . \quad (161)$$

This can be written as

$$\frac{\partial P}{\partial \tau} = \rho_F \frac{\partial}{\partial x} \left[ \frac{d\phi}{dx} P \right] + \rho_D \frac{\partial^2 P}{\partial x^2} , \quad (162)$$

where

$$\rho_F = \frac{qRTt^*}{\alpha^{*2}FM\gamma} , \quad (163)$$

$$\rho_D = \frac{Dt^*}{\alpha^{*2}} . \quad (164)$$

The parameters ( $\rho_F$  and  $\rho_D$ ) are dimensionless. We set  $\rho_D$  to unity to find a value for  $t^*$ .

Using parameters from table 5, introducing the molecular weight of the dye (548.77) and calculating the diffusion coefficient  $D$  from the Appendix ( $4.4 \cdot 10^{-10} \text{ m}^2/\text{s}$ ), we can solve the equation (165) in Matlab with

$$P_0 = \frac{1}{2} \left[ 1 + \cos \left[ \frac{\pi}{2} (x + 7) \right] \right] \text{ when } |x| < 20 \quad (165)$$

as initial condition ( $t = 0$ ) and assuming no flux limits in the far fields (at distance ten times further than the membrane length).  $P_0$  is set to approximate an initial peak of the dye in the extracellular area, which stands for the injection of the dye during the experiment.

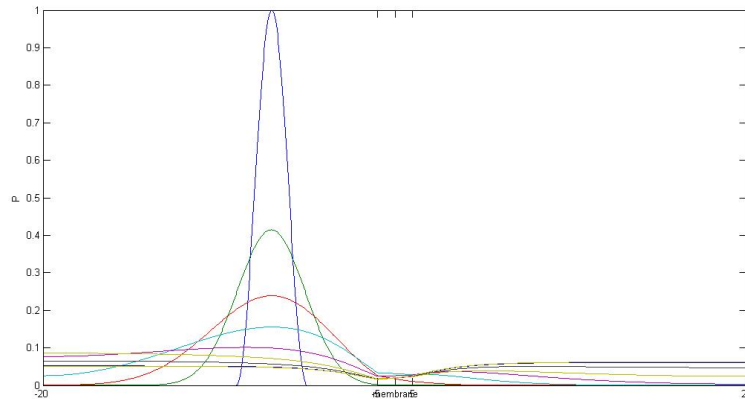


Figure 21: Distribution of the dye when  $\rho_F = \rho_D$

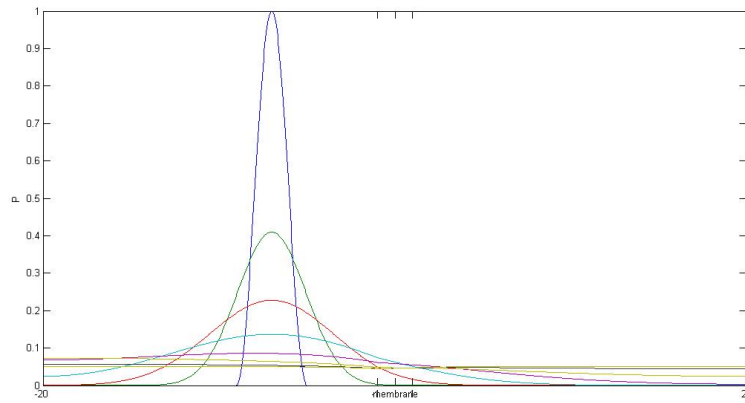


Figure 22: Distribution of the dye when  $\rho_F = 10\rho_D$

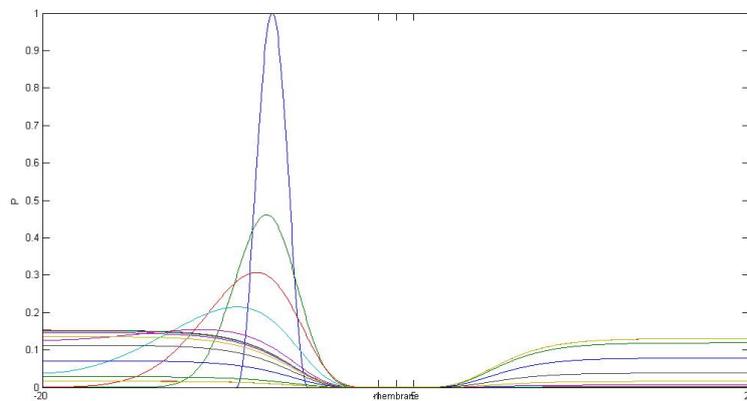


Figure 23: Distribution of the dye when  $\rho_F = 0.1\rho_D$

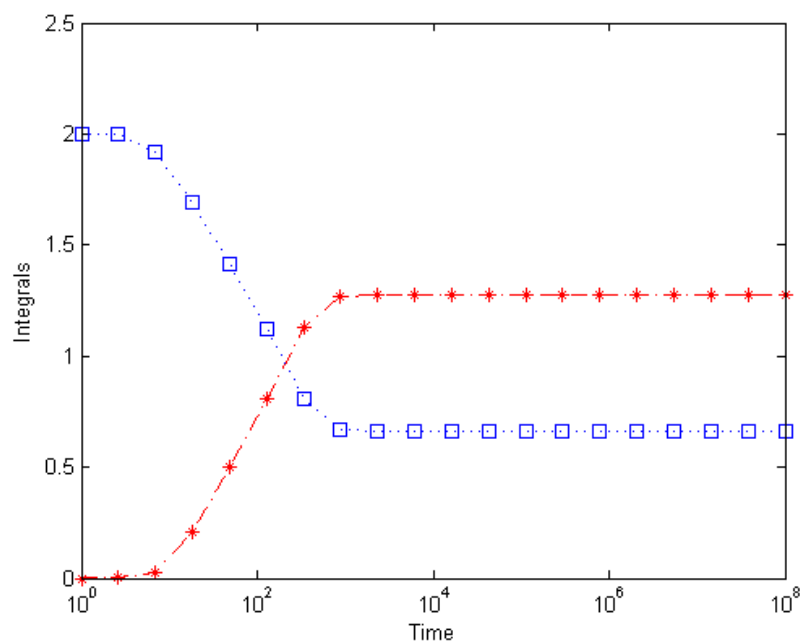


Figure 24: Distribution integrals versus time, where the red starred line stands for the dye distribution inside the cell and the blue squared line for the distribution outside the cell.

Figure 24 shows the mass distribution inside the cell versus time after integrating the values of figure 21. Note that the dye distribution outside the cell is decreased at the same rate as the distribution inside the cell increases. After some time, they both reach an equilibrium state. In the whole time, the sum of both lines remains constant.

### 4.3 Conclusions from modelling the experimental procedures

#### 4.3.1 Modelling valinomycin

It is obvious from the graphs in figures 17–20, that the system of valinomycin quickly reaches equilibrium. The addition of valinomycin affects the time needed for equilibrium in the way that the more valinomycin we add for certain amount of potassium concentration, the faster the system reaches equilibrium.

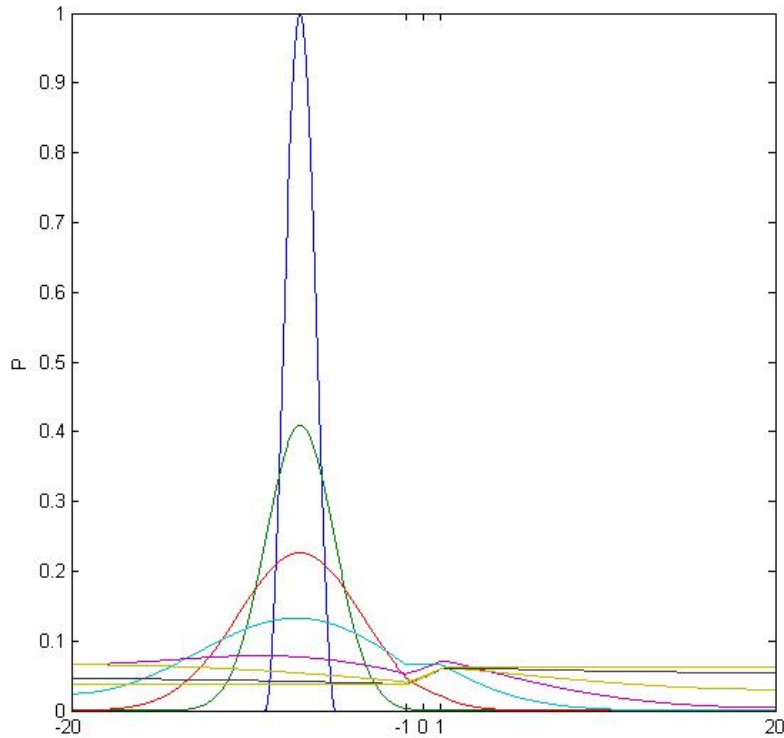


Figure 25: Distribution of the dye when the extracellular potassium concentration is 5 mM

#### 4.3.2 Potential modelling

From figures 21–23 it is obvious that the diffusion term and the potential term in the Fokker–Planck equation (165), both have an effect on the distribution of the dye molecule across the membrane. When these terms are of the same order, then we have figure 21. When this order changes, we can get from pure diffusion effect (Figure 22) to a more dominant electric field in the area of the membrane (Figure 23). In figure 23, the dye has less chance to be closer to the membrane. This is why we see a large area of empty space near the membrane. But once the molecule gets inside, it tends to pile up away from the membrane, due to repulsive forces from the membrane surface charge.

In the figures 25–28, we use the Fokker–Planck equation to simulate the dye distribution when we add different amount of potassium ions outside the cell.

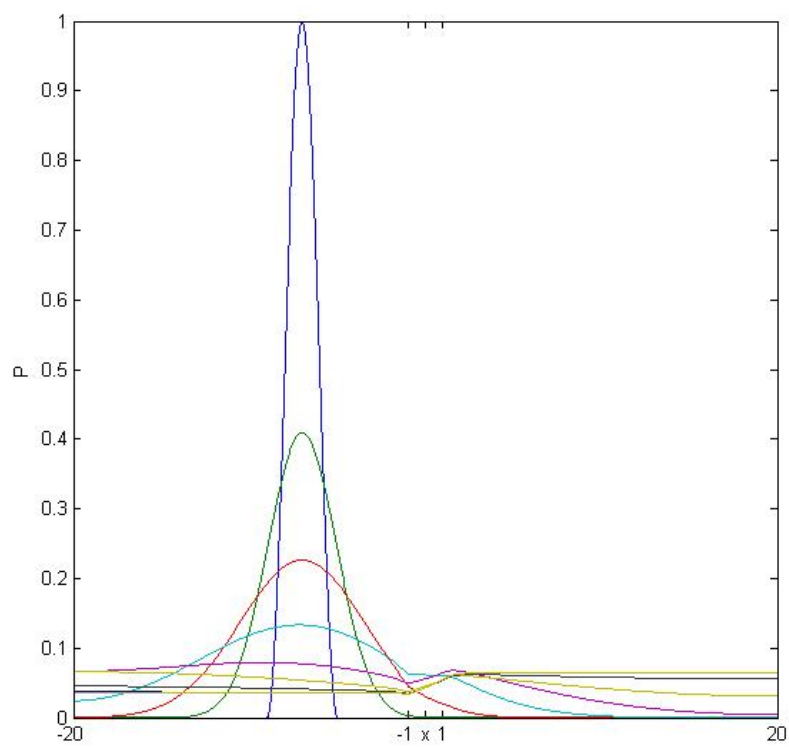


Figure 26: Distribution of the dye when the extracellular potassium concentration is 12 mM

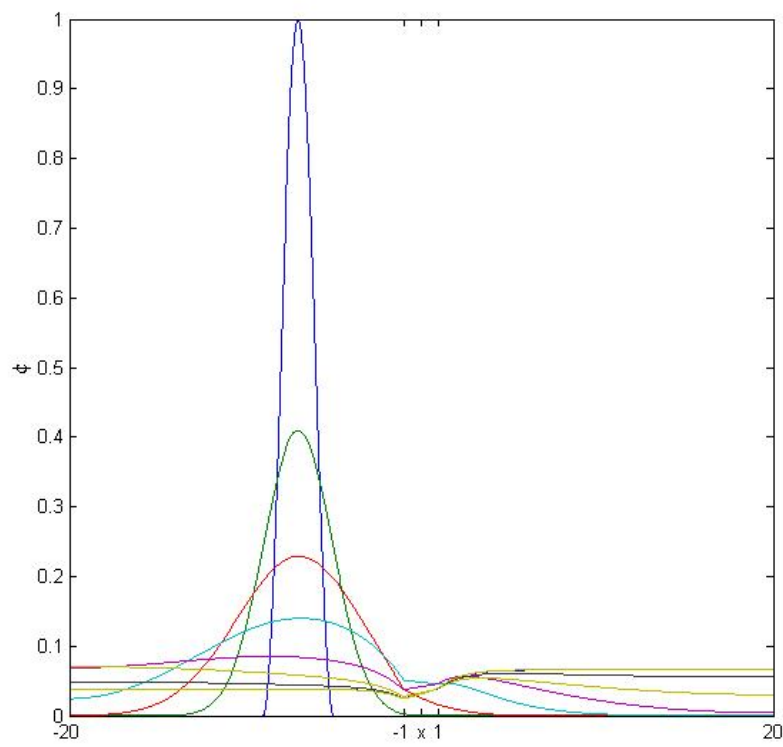


Figure 27: Distribution of the dye when the extracellular potassium concentration is 50 mM

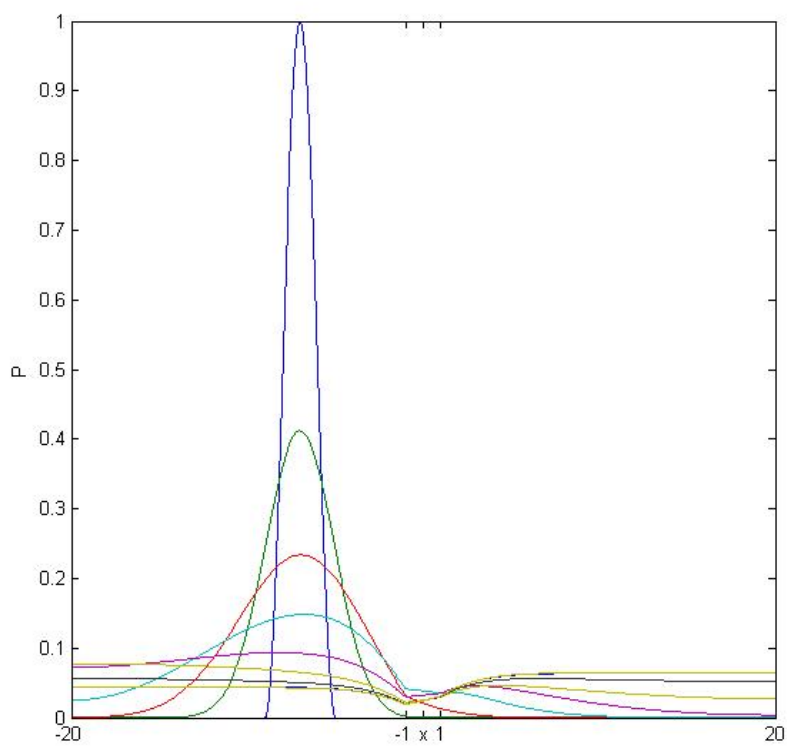


Figure 28: Distribution of the dye when the extracellular potassium concentration is 100 mM

## 5 CONCLUSIONS

In section 2, we described the experimental procedures performed. From these experiments, we concluded that the dye's motion can be affected by the addition of different amounts of valinomycin. Adding more valinomycin in the cellular environment means that the flux of potassium ions through the membrane is increased, altering the membrane potential at the same time. In other words, alterations in the membrane potential have a direct effect in the distribution of the dye. In general, this would mean that by altering the membrane potential, we are able to control the amount of foreign molecules getting inside the cell.

In the electrostatic part, we were able to predict the distribution of the potential inside and outside of the cell. Plus, according to our calculations we concluded that the pH of the cell does not affect the membrane potential, at least in a direct way. If there is a less direct way, there is still to be identify.

We also found that valinomycin reaches equilibrium approximately in 0.5 second, which is less than the incubation time we used in the experimental procedure. After the period of 0.5 second, there is a dynamic equilibrium in the system. This means that there is still conversion from the free form of valinomycin to the complex form, but the concentrations remain the same.

From chapter 4, we concluded that the valinomycin complex and free ion system comes to equilibrium relatively quickly, so no incubation period before the measurement of fluorescence is essential. As for the equations describing the probability of the dye to cross the membrane we can use the experimental data to simulate the distribution of the dye in the membrane vicinity. As the extracellular potassium concentration increases the distribution of the dye is decreases. In other words, the dye struggles more to cross the membrane. This is because the potential well within the membrane is getting deeper and the potassium transport is getting more difficult.

The mass conservation graphs present a theoretical prediction of what happens in the vicinity of the membrane during the experiment. The mass outside the cell starts to decrease, whereas the mass inside the cell increases as the time increases. This means that once the dye gets cross the obstacle of the potential well within the membrane, it is distributed within the cell. Actually, the shape of figure shape looks like the shape of curves from the experimental figures 6–10. However, in the experimental data presentation, the mass of the dye inside the cell does not reach an equilibrium within the measurement time. This can be due to experimental conditions such as inability of the machine to properly detect changes in the fluorescence of the signal.

To conclude, we were able to demonstrate and explain an experimental procedure both physically (Chapter 2) and mathematically (Chapter 4), and by using simple mathematical approximations (Chapters 3 and 4), we predicted the distribution of a molecule in the cell when this molecule is introduced in the extracellular environment and is subjected to electrostatic forces. This prediction is close enough to the data driven by the experiments.

Substance	Molecular Weight	D(cm <sup>2</sup> /s)
hydrogen	1	4.5 10 <sup>-5</sup>
oxygen	32	2.1 10 <sup>-5</sup>
carbon dioxide	48	1.92 10 <sup>-5</sup>
glucose	192	6.60 10 <sup>-6</sup>
insulin	5734	2.10 10 <sup>-6</sup>
cytochrome c	13370	1.14 10 <sup>-6</sup>
myoglobin	16900	5.1 10 <sup>-7</sup>
serum albumin	66500	6.03 10 <sup>-7</sup>
hemoglobin	64500	6.9 10 <sup>-7</sup>
catalase	247500	4.1 10 <sup>-7</sup>
urease	482700	3.46 10 <sup>-7</sup>
fibrinogen	330000	1.97 10 <sup>-7</sup>
myosin	524800	1.05 10 <sup>-5</sup>
tobacco mosaic virus	40590000	5.3 10 <sup>-8</sup>

Table 8: Molecular weight of certain substances and their diffusion coefficients [39]

## APPENDIX

There is no literature for the diffusion coefficient of DiSBAC<sub>4</sub>(3). We can only find the diffusion coefficients for a limit number of biological substances [39]. From plotting these values (Table 8) in respect to their molecular weight, we get figure **30** where we see that the values for the diffusion coefficient

$$y = 7210.2x^{-0.442} \quad (166)$$

where  $x$  stands for the molecular weight of the molecule and  $y$  for the diffusion coefficient in cm<sup>2</sup>/s. The exact value of the diffusion coefficient equals to 10<sup>-8</sup> of  $y$ .

For DiSBAC<sub>4</sub>(3), the molecular weight is 548.77 and by using the equation (166) we get the diffusion coefficient 443.75\*10<sup>-12</sup> m<sup>2</sup>/s.

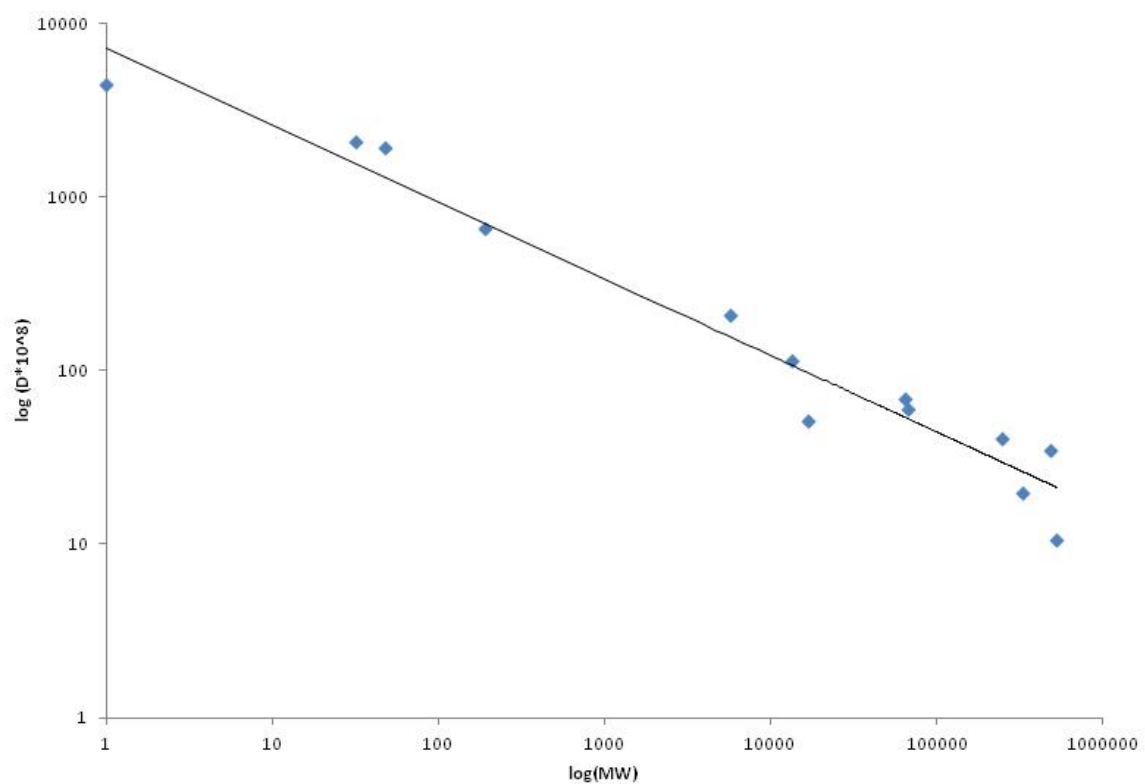


Figure 29: Diffusion coefficients vs molecular weight of substances in Table 8[39]

## References

- [1] B. Alberts, A. Johnson, J. Lewis, M. Raff, K. Roberts, and P. Walter. Molecular biology of the cell. *New York: Garland Science*, 2002.
- [2] D. Andelman. Electrostatic Properties of Membranes: The Poisson-Boltzmann Theory. *Handbook of Biological Physics*, 1:603–641, 1995.
- [3] M.Z. Bazant, K. Thornton, and A. Ajdari. Diffuse-charge dynamics in electrochemical systems. *Physical Review E*, 70(2):021506, 2004.
- [4] M. Bechem, S. Beutner, N. Burkhardt, C. Fuchs, C. Kryschi, W. Paffhausen, B. Reiffers, A. Schade, W.R. Schlue, D. Schmid, et al. Novel hyperpolarizable and fluorescent dyes in lipid membranes: studying membrane potentials using nonlinear optical and fluorescence. *Electrochimica Acta*, 48(20-22):3387–3393, 2003.
- [5] M.J. Borgnia, G.D. Eytan, and Y.G. Assaraf. Competition of Hydrophobic Peptides, Cytotoxic Drugs, and Chemosensitizers on a Common P-glycoprotein Pharmacophore as Revealed by Its ATPase Activity. *Journal of Biological Chemistry*, 271(6):3163–3171, 1996.
- [6] P. Borst and R.O. Elferink. Mammalian abc transporters in health and disease. *Annual review of biochemistry*, 71(1):537–592, 2002.
- [7] P.G. Bray, S.R. Hawley, M. Mungthin, and S.A. Ward. Physicochemical Properties Correlated with Drug Resistance and the Reversal of Drug Resistance in *Plasmodium falciparum*. *Molecular pharmacology*, 50(6):1556–1559, 1996.
- [8] E. Brunner. Theorie der reaktionsgeschwindigkeit in heterogenen systemen. *Zeitschrift fr Physikalische Chemie*, 47:56–102, 1904.
- [9] E. Brunner. Die kathodische und anodische stromspannungs-kurve bei der elektrolyse von jod-jodkaliumlösungen. *Zeitschrift fr Physikalische Chemie*, 58(1):1–127, 1907.

- [10] M. Castaing, A. Loiseau, and M. Dani. Designing multidrug-resistance modulators circumventing the reverse ph gradient in tumours. *Journal of pharmacy and pharmacology*, 53(7):1021–1028, 2001.
- [11] G. Cevc. Membrane electrostatics. *Biochimica et biophysica acta*, 1031(3):311–382, 1990.
- [12] X. Chang. A molecular understanding of atp-dependent solute transport by multidrug resistance-associated protein mrp1. *Cancer and Metastasis Reviews*, 26(1):15–37, 2007.
- [13] D.L. Chapman. LI. A contribution to the theory of electrocapillarity. *Philosophical Magazine Series 6*, 25(148):475–481, 1913.
- [14] D. Chowdhury. Molecular motors: Design, mechanism, and control. *Computing in Science & Engineering*, 10(2):70–77, 2008.
- [15] C.E. Cooper, D. Bruce, and P. Nicholls. Use of oxonol v as a probe of membrane potential in proteoliposomes containing cytochrome oxidase in the submitochondrial orientation. *Biochemistry*, 29(16):3859–3865, 1990.
- [16] C.A. Dise and D.B. Goodman. The relationship between valinomycin-induced alterations in membrane phospholipid fatty acid turnover, membrane potential, and cell volume in the human erythrocyte. *Journal of Biological Chemistry*, 260(5):2869–2874, 1985.
- [17] M. Faraday. Experimental researches in electricity.—seventh series. *Philosophical Transactions of the Royal Society of London*, 124:77–122, 1834.
- [18] M.S. Fernandez and P. Fromherz. Lipoid ph indicators as probes of electrical potential and polarity in micelles. *The Journal of Physical Chemistry*, 81(18):1755–1761, 1977.
- [19] J. Ferté. Analysis of the tangled relationships between P-glycoprotein-mediated multidrug resistance and the lipid phase of the cell membrane. *European Journal of Biochemistry*, 267(2):277–294, 2000.

- [20] C. Fleck, R.R. Netz, and H.H. Von Grünberg. Poisson-Boltzmann theory for membranes with mobile charged lipids and the pH-dependent interaction of a DNA molecule with a membrane. *Biophysical journal*, 82(1):76–92, 2002.
- [21] K.E. Forsten, R.E. Kozack, D.A. Lauffenburger, and S. Subramaniam. Numerical solution of the nonlinear Poisson-Boltzmann equation for a membrane-electrolyte system. *The Journal of Physical Chemistry*, 98(21):5580–5586, 1994.
- [22] TD Frank, PJ Beek, and R. Friedrich. Fokker-planck perspective on stochastic delay systems: Exact solutions and data analysis of biological systems. *Physical Review E*, 68(2):021912, 2003.
- [23] F. Frezard and A. Garnier-Suillerot. Comparison of the membrane transport of anthracycline derivatives in drug-resistant and drug-sensitive k562 cells. *European journal of biochemistry*, 196(2):483–491, 1991.
- [24] D. Gillespie, W. Nonner, and R.S. Eisenberg. Coupling poisson–nernst–planck and density functional theory to calculate ion flux. *Journal of Physics: Condensed Matter*, 14:12129–12145, 2002.
- [25] K. Goda, L. Balkay, T. Márián, L. Trón, A. Aszalós, and G. Szabó. Intracellular pH does not affect drug extrusion by P-glycoprotein. *Journal of Photochemistry and Photobiology B: Biology*, 34(2-3):177–182, 1996.
- [26] J.E. González, K. Oades, Y. Leychkis, A. Harootunian, and P.A. Negulescu. Cell-based assays and instrumentation for screening ion-channel targets. *Drug Discovery Today*, 4(9):431–439, 1999.
- [27] J.E. González and R.Y. Tsien. Voltage sensing by fluorescence resonance energy transfer in single cells. *Biophysical journal*, 69(4):1272–1280, 1995.
- [28] M.M. Gottesman. Mechanisms of cancer drug resistance. *Annual review of medicine*, 53(1):615–627, 2002.

- [29] M.M. Gottesman and I. Pastan. Biochemistry of multidrug resistance mediated by the multidrug transporter. *Annual review of biochemistry*, 62(1):385–427, 1993.
- [30] G. Gouy. Sur la constitution de la charge électronique a la surface d’un électrolyte. *Journal de physique*, 9(4):457–467, 1910.
- [31] D.C. Grahame. The electrical double layer and the theory of electrocapillarity. *Chemical Reviews*, 41(3):441–501, 1947.
- [32] Z. Gucheng, W. Hao, X. Yanfang, S. Jintao, P. Yunlong, and C. Jiye. Quantum dots uptake by K562 cells visualized through atomic force microscopy. *Chemical Journal on Internet*, 2005.
- [33] H.V. Helmholtz. Studien uber electrische grenzschichten. *Annual Review of Physical Chemistry*, 7:337–382, 1879.
- [34] C.F. Higgins. Multiple molecular mechanisms for multidrug resistance transporters. *Nature*, 446:749–757, 2007.
- [35] S.B. Hladky, J.C. Leung, and W.J. Fitzgerald. The mechanism of ion conduction by valinomycin: analysis of charge pulse responses. *Biophysical journal*, 69:1758–1772, 1995.
- [36] M.M. Hoffman, L.Y. Wei, and P.D. Roepe. Are altered pHi and membrane potential in hu MDR 1 transfectants sufficient to cause MDR protein-mediated multidrug resistance? *The Journal of General Physiology*, 108:295–313, 1996.
- [37] Y. Huang and W. Sadée. Membrane transporters and channels in chemoresistance and –sensitivity of tumor cells. *Cancer letters*, 239:168–182, 2006.
- [38] T. Kanamaru, T. Horita, and Y. Okabe. Theoretical analysis of array-enhanced stochastic resonance in the diffusively coupled fitzhugh-nagumo equation. *Physical Review E*, 64(3):031908, 2001.
- [39] J. Keener and J. Sneyd. *Mathematical Physiology: Cellular Physiology*. Springer Verlag, 2008.

- [40] H. Kim, M. Barroso, R. Samanta, L. Greenberger, and E. Sztul. Experimentally induced changes in the endocytic traffic of p-glycoprotein alter drug resistance of cancer cells. *American Physiological Society*, 273(2):C687–C702, 1997.
- [41] J.A. Kloepfer, N. Cohen, and J.L. Nadeau. FRET between CdSe quantum dots in lipid vesicles and water- and lipid-soluble dyes. *The Journal of Physical Chemistry B*, 108(44):17042–17049, 2004.
- [42] M.K. Koo, C.H. Oh, A.L. Holme, and S. Pervaiz. Simultaneous analysis of steady-state intracellular pH and cell morphology by automated laser scanning cytometry. *Cytometry Part A*, 71(2):87–93, 2007.
- [43] Z. Krasznai, T. Márián, H. Izumi, S. Damjanovich, L. Balkay, L. Trón, and M. Morisawa. Membrane hyperpolarization removes inactivation of Ca<sup>2+</sup> channels, leading to Ca<sup>2+</sup> influx and subsequent initiation of sperm motility in the common carp. *Proceedings of the National Academy of Sciences*, 97(5):2052–2057, 2000.
- [44] R. Krishna and L.D. Mayer. Multidrug resistance (MDR) in cancer: Mechanisms, reversal using modulators of MDR and the role of MDR modulators in influencing the pharmacokinetics of anticancer drugs. *European Journal of Pharmaceutical Sciences*, 11(4):265–283, 2000.
- [45] A. Kuznetsov, V.P. Bindokas, J.D. Marks, and L.H. Philipson. FRET-based voltage probes for confocal imaging: membrane potential oscillations throughout pancreatic islets. *American Journal of Physiology-Cell Physiology*, 289(1):224–229, 2005.
- [46] J. Lacroix, M. Poet, L. Huc, V. Morello, N. Djerbi, M. Ragno, M. Rissel, X. Tekpli, P. Gounon, D. Lagadic-Gossmann, and L. Counillon. Kinetic analysis of the regulation of the Na<sup>+</sup>/H<sup>+</sup> exchanger nHE-1 by osmotic shocks. *Biochemistry*, 47(51):13674–13685, 2008.

- [47] H. Lage. ABC-transporters: implications on drug resistance from microorganisms to human cancers. *International journal of antimicrobial agents*, 22(3):188–199, 2003.
- [48] A.K. Larsen, A.E. Escargueil, and A. Skladanowski. Resistance mechanisms associated with altered intracellular distribution of anticancer agents. *Pharmacology & Therapeutics*, 85(3):217–229, 2000.
- [49] D. Lautier, Y. Canitrot, R.G. Deeley, and S.P.C. Cole. Multidrug resistance mediated by the multidrug resistance protein (MRP) gene. *Biochemical pharmacology*, 52(7):967–977, 1996.
- [50] X. Liang and Y. Huang. Physical state changes of membrane lipids in human lung adenocarcinoma a549 cells and their resistance to cisplatin. *The International Journal of Biochemistry & Cell Biology*, 34(10):1248–1255, 2002.
- [51] X.J. Liang, J.J. Yin, J.W. Zhou, P.C. Wang, B. Taylor, C. Cardarelli, M. Kozar, R. Forte, A. Aszalos, and M.M. Gottesman. Changes in biophysical parameters of plasma membranes influence cisplatin resistance of sensitive and resistant epidermal carcinoma cells. *Experimental cell research*, 293(2):283–291, 2004.
- [52] A.D. MacGillivray. Nernst–planck equations and the electroneutrality and donnan equilibrium assumptions. *The Journal of Chemical Physics*, 48(7):2903–2907, 1968.
- [53] M. Mandala, G. Serck-Hanssen, G. Martino, and K.B. Helle. The fluorescent cationic dye rhodamine 6g as a probe for membrane potential in bovine aortic endothelial cells. *Analytical biochemistry*, 274(1):1–6, 1999.
- [54] C. Martin, G. Berridge, P. Mistry, C. Higgins, P. Charlton, and R. Callaghan. Drug Binding Sites on P-Glycoprotein Are Altered by ATP Binding Prior to Nucleotide Hydrolysis. *Biochemistry*, 39:11901–11906, 2000.
- [55] R. Martínez-Zaguilán, N. Raghunand, R.M. Lynch, W. Bellamy, G.M. Martinez, B. Rojas, D. Smith, W.S. Dalton, and R.J. Gillies. pH and drug

- resistance. I. Functional expression of plasmalemmal V-type H<sup>+</sup>-ATPase in drug-resistant human breast carcinoma cell lines. *Biochemical pharmacology*, 57(9):1037–1046, 1999.
- [56] S. McLaughlin. The electrostatic properties of membranes. *Annual review of biophysics and biophysical chemistry*, 18(1):113–136, 1989.
- [57] S. McLaughlin and M. Eisenberg. Antibiotics and membrane biology. *Annual Review of Biophysics and Bioengineering*, 4(1):335–366, 1975.
- [58] K. Mouri and T. Shimokawa. The fokker-planck approach for the cooperative molecular motor model with finite number of motors. *Biosystems*, 93(1-2):58–67, 2008.
- [59] E. Munteanu, M. Verdier, F. Grandjean-Forestier, C. Stenger, C. Jayat-Vignoles, S. Huet, J. Robert, and M.H. Ratinaud. Mitochondrial localization and activity of p-glycoprotein in doxorubicin-resistant k562 cells. *Biochemical pharmacology*, 71(8):1162–1174, 2006.
- [60] C.C. Murdock and E.E. Zimmerman. Polarization impedance at low frequencies. *Physics*, 7(6):211–219, 1936.
- [61] W. Nernst. Theorie der reaktionsgeschwindigkeit in heterogenen systemen. *Zeitschrift fr Physikalische Chemie*, 47(1):52–55, 1904.
- [62] T. Ohira and Y. Sato. Resonance with noise and delay. *Physical Review Letters*, 82(14):2811–2815, 1999.
- [63] G.S. Ohm. *Bestimmung des Gesetzes, nach welchem Metalle die Kontaktelektricität leiten: Nebst einem Entwurfe zur einer Theorie des Voltaschen Apparates und des Schweiggerschen Multiplcators*. Journal für Chemie und Physik, 1826.
- [64] H. Ohshima and S. Ohki. Donnan potential and surface potential of a charged membrane. *Biophysical journal*, 47(5):673–678, 1985.

- [65] M. Otto. Looking toward basic science for potential drug discovery targets against community-associated MRSA. *Medicinal Research Reviews*, 30(1):1–22, 2010.
- [66] Z. Ouar, R. Lacave, M. Bens, and A. Vandewalle. Mechanisms of altered sequestration and efflux of chemotherapeutic drugs by multidrug-resistant cells. *Cell biology and toxicology*, 15(2):91–100, 1999.
- [67] I.T. Paulsen, M.H. Brown, and R.A. Skurray. Proton-dependent multidrug efflux systems. *Microbiological Reviews*, 60(4):575–608, 1996.
- [68] S.A. Peel. The abc transporter genes of plasmodium falciparum and drug resistance. *Drug Resistance Updates*, 4(1):66–74, 2001.
- [69] R. Perry and D. Green. Perrys Chemical Engineers Handbook (7th edn.) McGraw-Hill. *New York, USA*, 1998.
- [70] R. Phillips, J. Kondev, J. Theriot, N. Orme, and H. Garcia. *Physical biology of the cell*. Garland Science, 2009.
- [71] L.J.V. Piddock. Multidrug-resistance efflux pumps? not just for resistance. *Nature Reviews Microbiology*, 4(8):629–636, 2006.
- [72] J. Plásek and K. Sigler. Slow fluorescent indicators of membrane potential: a survey of different approaches to probe response analysis. *Journal of Photochemistry and Photobiology B: Biology*, 33(2):101–124, 1996.
- [73] A. Priplata, J. Niemi, M. Salen, J. Harry, L.A. Lipsitz, and JJ Collins. Noise-enhanced human balance control. *Physical Review Letters*, 89(23):238101, 2002.
- [74] A.D. Purdon and S.I. Rapoport. Energy requirements for two aspects of phospholipid metabolism in mammalian brain. *Biochemical Journal*, 335(Pt 2):313, 1998.
- [75] N. Raghunand, R. Martínez-Zaguilán, S.H. Wright, and R.J. Gillies. ph and

- drug resistance. ii. turnover of acidic vesicles and resistance to weakly basic chemotherapeutic drugs. *Biochemical pharmacology*, 57(9):1047–1058, 1999.
- [76] C. Rauch. On the relationship between drugs size, cell membrane mechanical properties and high levels of multi drug resistance: a comparison to published data. *European Biophysics Journal*, 38(4):537–546, 2009.
- [77] C. Rauch and A. Pluen. Multi drug resistance-dependent vacuum cleaner functionality potentially driven by the interactions between endocytosis, drug size and Pgp-like transporters surface density. *European Biophysics Journal*, 36(2):121–131, 2007.
- [78] R. Regev and G.D. Eytan. Flip–flop of doxorubicin across erythrocyte and lipid membranes. *Biochemical pharmacology*, 54(10):1151–1158, 1997.
- [79] G. Richardson. A multiscale approach to modelling electrochemical processes occurring across the cell membrane with application to transmission of action potentials. *Mathematical Medicine and Biology*, 2009.
- [80] G. Richardson and J.R. King. Time-dependent modelling and asymptotic analysis of electrochemical cells. *Journal of Engineering Mathematics*, 59(3):239–275, 2007.
- [81] P.D. Roepe. The P-glycoprotein efflux pump: how does it transport drugs? *The Journal of membrane biology*, 166(1):71–73, 1998.
- [82] P.D. Roepe and J.A. Martiney. Are ion-exchange processes central to understanding drug-resistance phenomena? *Trends in pharmacological sciences*, 20(2):62–65, 1999.
- [83] P.D. Roepe, L.Y. Wei, J. Cruz, and D. Carlson. Lower electrical membrane potential and altered pHi homeostasis in multidrug-resistant (MDR) cells: further characterization of a series of MDR cell lines expressing different levels of P-glycoprotein. *Biochemistry*, 32(41):11042–11056, 1993.

- [84] I. Rouzina and V.A. Bloomfield. Macroion attraction due to electrostatic correlation between screening counterions. 1. Mobile surface-adsorbed ions and diffuse ion cloud. *Journal of Physical Chemistry*, 100(23):9977–9989, 1996.
- [85] C.T. Santai, F. Fritz, and P.D. Roepe. ARTICLES-Effects of Ion Gradients on H<sup>+</sup> Transport Mediated by Human MDR 1 Protein. *Biochemistry-Columbus*, 38(13):4227–4234, 1999.
- [86] M. Schienbein, K. Franke, and H. Gruler. Random walk and directed movement: comparison between inert particles and self-organized molecular machines. *Physical Review E*, 49(6):5462, 1994.
- [87] M. Schienbein and H. Gruler. Enzyme kinetics, self-organized molecular machines, and parametric resonance. *Physical Review E*, 56(6):7116, 1997.
- [88] R.B. Schoch, J. Han, and P. Renaud. Transport phenomena in nanofluidics. *Reviews of Modern Physics*, 80(3):839–883, 2008.
- [89] R.B. Schoch, H. Van Lintel, and P. Renaud. Effect of the surface charge on ion transport through nanoslits. *Physics of Fluids*, 17:100604, 2005.
- [90] J.K. Seydel and M. Wiese. *Drug-membrane interactions: analysis, drug distribution, modeling*. Vch Verlagsgesellschaft Mbh, 2002.
- [91] V. Sharma and D. Piwnica-Worms. Metal complexes for therapy and diagnosis of drug resistance. *Chemical reviews*, 99(9):2545–2560, 1999.
- [92] F.J. Sharom. Shedding light on drug transport: structure and function of the p-glycoprotein multidrug transporter (abcb1) . *Biochemistry and cell biology*, 84(6):979–992, 2006.
- [93] F.J. Sharom, M.R. Lugo, and P.D.W. Eckford. New insights into the drug binding, transport and lipid flippase activities of the p-glycoprotein multidrug transporter. *Journal of bioenergetics and biomembranes*, 37(6):481–487, 2005.
- [94] J.A. Sheps and V. Ling. Preface: the concept and consequences of multidrug resistance. *European Journal of Physiology*, 453(5):545–553, 2007.

- [95] S. Simon, D. Roy, and M. Schindler. Intracellular pH and the control of multidrug resistance. *Proceedings of the National Academy of Sciences*, 91(3):1128–1132, 1994.
- [96] A. Singer, D. Gillespie, J. Norbury, and R.S. Eisenberg. Singular perturbation analysis of the steady-state poisson–nernst–planck system: Applications to ion channels. *European journal of applied mathematics*, 19(5):541–560, 2008.
- [97] A. Singer and J. Norbury. A poisson–nernst–planck model for biological ion channels - an asymptotic analysis in a 3–d narrow funnel. *Journal of Applied Mathematics*, 70(3):949–968, 2009.
- [98] S.J. Singer and G.L. Nicolson. The fluid mosaic model of the structure of cell membranes. *Science*, 175(23):720–731, 1972.
- [99] G. Spach. *Physical chemistry of transmembrane ion motions: proceedings of the 36th International Meeting of the Société de chimie physique, Paris, 27 September-1 October 1982*, volume 24. Elsevier Publishing Company, 1983.
- [100] G. Stark, B. Ketterer, R. Benz, and P. Läuger. The rate constants of valinomycin-mediated ion transport through thin lipid membranes. *Biophysical Journal*, 11(12):981–994, 1971.
- [101] Z. Stern. *Elektrochem.* 30. *View Record in Scopus— Cited By in Scopus (1)*, page 508, 1924.
- [102] N.G. van Kampen. *Stochastic processes in physics and chemistry*. North Holland, 2007.
- [103] C.F. Varley. Polarization of metallic surfaces in aqueous solutions. on a new method of obtaining electricity from mechanical force, and certain relations between electro-static induction and the decomposition of water. *Philosophical Transactions of the Royal Society of London*, 161:129–136, 1871.
- [104] A. Volta. On the electricity excited by the mere contact of conducting substances of different kinds. In *Abstracts of the Papers Printed in the Philo-*

*sophical Transactions of the Royal Society of London*, volume 1, pages 27–29. JSTOR, 1800.

- [105] A.S. Waggoner. Dye indicators of membrane potential. *Annual review of biophysics and bioengineering*, 8:47–68, 1979.
- [106] H.S.V. Walraven, M.J.C. Scholts, S.D. Zakharov, R. Kraayenhof, and R.A. Dilley. pH-dependent  $\text{Ca}^{2+}$  binding to the  $\text{F}_0\text{F}_1$ -subunit affects proton translocation of the atp synthase from *synechocystis* 6803. *Journal of bioenergetics and biomembranes*, 34(6):455–464, 2002.
- [107] K. Wiesenfeld and F. Moss. Stochastic resonance and the benefits of noise: from ice ages to crayfish and squids. *Nature*, 373(6509):33–36, 1995.
- [108] J.J. Wright and D.T.J. Liley. Simulation of electrocortical waves. *Biological Cybernetics*, 72(4):347–356, 1995.
- [109] A. Yamada, N. Gaja, S. Ohya, K. Muraki, H. Narita, T. Ohwada, and Y. Imaizumi. Full Papers-Usefulness and Limitation of DiBAC4 (3), a Voltage-Sensitive Fluorescent Dye, for the Measurement of Membrane Potentials Regulated by Recombinant Large Conductance  $\text{Ca}^{2+}$ -Activated  $\text{K}^{+}$ . *Japanese Journal of Pharmacology*, 86(3):342–350, 2001.
- [110] E.E. Zimmerman. The influence of temperature of polarization capacity and resistance. *Physical Review*, 35(5):543, 1930.